Mathematical model for the effects of adhesion and mechanics on cell migration speed

Paul A. DiMilla,* Kenneth Barbee,‡ and Douglas A. Lauffenburger§

Departments of *Chemical Engineering and ‡Bioengineering, University of Pennsylvania, Philadelphia, Pennsylvania 19104; and §Departments of Chemical Engineering and Cell and Structural Biology, University of Illinois at Urbana-Champaign, Urbana, Illinois 61801 USA

ABSTRACT Migration of mammalian blood and tissue cells over adhesive surfaces is apparently mediated by specific reversible reactions between cell membrane adhesion receptors and complementary ligands attached to the substratum. Although in a number of systems these receptors and ligand molecules have been isolated and identified, a theory capable of predicting the effects of their properties on cell migration behavior currently does not exist.

We present a simple mathematical model for elucidating the dependence of cell speed on adhesion-receptor/ligand binding and cell mechanical properties. Our model can be applied to propose answers to questions such as: does an optimal adhesiveness exist for cell movement? How might changes in receptor and ligand density and/or affinity affect the rate of migration? Can cell rheological properties influence movement speed?

This model incorporates cytoskeletal force generation, cell polarization, and dynamic adhesion as requirements for persistent cell movement. A critical feature is the proposed existence of an asymmetry in some cell adhesion-receptor property, correlated with cell polarity. We consider two major alternative mechanisms underlying this asymmetry: (*a*) a spatial distribution of adhesion-receptor number due to polarized endocytic trafficking and (*b*) a spatial variation in adhesion-receptor/ligand bond strength. Applying a viscoelastic-solid model for cell mechanics allows us to represent one-dimensional locomotion with a system of differential equations describing cell deformation and displacement along with adhesion-receptor dynamics. In this paper, we solve these equations under the simplifying assumption that receptor dynamics are at a quasi-steady state relative to cell locomotion. Thus, our results are strictly valid for sufficiently slow cell movement, as typically observed for tissue cells such as fibroblasts.

Numerical examples relevant to experimental systems are provided. Our results predict how cell speed might vary with intracellular contractile force, cell rheology, receptor/ligand kinetics, and receptor/ligand number densities. A biphasic dependence is shown to be possible with respect to some of the system parameters, with position of the maxima essentially governed by a balance between transmitted contractile force and adhesiveness. We demonstrate that predictions for the two alternative asymmetry mechanisms can be distinguished and could be experimentally tested using cell populations possessing different adhesion-receptor numbers.

INTRODUCTION

Mammalian blood and tissue cell migration is a complex phenomenon, depending on coordinated interactions among a number of underlying biochemical and biophysical processes. Much information has been obtained at the molecular level about the identity and properties of components involved in these processes, especially receptor-mediated adhesion to extracellular matrix ligands (Buck and Horwitz, 1987) and cytoskeletal force generation (Stossel et al., 1985), as well as at the overall cell behavioral level (Lackie, 1986; Devreotes and Zigmond, 1988). The purpose of this present work is to analyze cell behavioral observations based on cellular- and molecular-level properties using a mathematical model which provides a quantitative description of plausible mechanistic hypotheses.

Three general requirements for persistent cell movement have been identified: migrating cells adhere dynamically with their environment, generate the force necessary for propulsion by contraction of cytoskeletal elements, and are morphologically polarized in direction. Adhesion in many systems is primarily mediated by cell surface receptors known as integrins, 140 kDa heterodimers composed of α and β subunits (Buck and Horwitz, 1987; Hynes, 1987). Integrins bind reversibly to extracellular matrix protein ligands, such as fibronectin (Fn) and laminin (Ln), which contain distinct cell-binding domains (Ruoslahti and Pierschbacher, 1987).

With few exceptions, actively motile cells require a dynamic contractile apparatus consisting of cytoskeletal elements, such as actin filaments, which may generate a

Address correspondence to Dr. Douglas A. Lauffenburger, Department of Chemical Engineering, University of Illinois at Urbana-Champaign, Roger Adams Laboratory, Urbana, IL 61801.

propulsive force upon polymerization and a tensile force by contracting (Lackie, 1986). Although the components involved in transmission of force from the contractile apparatus to the underlying substratum are not precisely known, the integrins are attractive candidates, as some studies have suggested that these molecules may be linked to the cytoskeleton through a series of intermediates (Burridge et al., 1988; Mueller et al., 1989). Cytoskeletal and cell surface organization is also important: in stationary cells integrins tend to cluster into focal contacts and stress fibers of bundled actin filaments are abundant. These stress fibers often terminate at focal contacts. In contrast, actively migrating cells tend to exhibit an absence of focal contacts and stress fibers, with a more diffuse, mesh-like cytoskeleton (Duband et al., 1988*b*). Finally, the coordinate orientation of the nucleus, microtubule-organizing center, and Golgi apparatus may define a direction for polarization in at least some cell types (Gotlieb et al., 1981; Singer and Kupfer, 1986).

Intuitively, three regimes of motile and adhesive behavior can be envisaged for a cell interacting with a surface. On a poorly adhesive surface a cell may stick so weakly that no traction is obtained and no net movement occurs. Alternatively, a cell may attach to a highly adhesive surface so strongly that it becomes immobilized. With an optimum balance of adhesive forces, however, the cell may be mobile (Lackie and Wilkinson, 1984). Both Carter (1965) and Harris (1973) used this hypothesis to interpret the preferential movement of murine fibroblasts from hydrophobic toward more hydrophillic surfaces. Dembo et al. (1981) developed a theoretical model to examine the role of adhesion receptor distribution on leukocyte movement speed, but their analysis neither predicted the effect of variations in cell-substratum adhesiveness on cell speed nor explained how an intracellular contractile force might be transmitted to produce an effective traction force. Although understanding of cell rheological properties has increased tremendously in recent years with the development of micropipette aspiration (Evans and Yeung, 1989; Skalak et al., 1988) and cell poking (Zahalak et al., 1990), a framework to couple adhesive and deformational events has remained lacking.

Our model is based on a chronological picture of a cell migration cycle, observed for in vitro locomotion over two-dimensional substrata, consisting of stages of lamellipodal extension, cytoskeletal contraction, and relaxation (Lackie, 1986; Trinkaus, 1984). It describes the cell's cytoskeleton as a simple network of viscoelastic and contractile elements, relating intracellular forces to substratum traction forces mediated by adhesion-receptor bonds with substratum ligands. A crucial aspect of the model is that net translocation of the cell requires an asymmetry in the cell/substratum interaction. At least two alternative mechanisms for generating such an asymmetry have been previously proposed: spatial distribution of cell surface adhesion-receptors (Bretscher, 1984) and spatial variation of adhesion-receptor/ligand affinity (Grinnell, 1986). We examine both of these possibilities.

We focus on one particular experimentally addressable characteristic of cell locomotion, cell movement speed, by considering a one-dimensional representation of a cell. Our model can predict how this commonly measured quantity may be influenced by key mechanistic parameters characterizing basic cell biochemical and biophysical properties. Further, we restrict ourselves here to cell motile behavior on uniform surfaces and analyze for possible effects of adhesion and mechanics on slower moving tissue cells, such as fibroblasts and endothelial cells. A corresponding analysis for faster moving white blood cells, such as neutrophils, will be the subject of future work.

GLOSSARY

A	cross-sectional area (cm^2)
c	viscosity (dyn-s/cm)
D_r	free receptor diffusivity (cm^2/s)
E	Young's modulus (dyn/cm^2)
f_c	dimensionless force, Eq. A12
F	intracellular contractile force (dyn)
G	modulus of rigidity (dyn/cm^2)
k	Hookean spring constant (dyn/cm)
k_b	Boltzman constant (erg/molecule-K)
k_e	endocytosis rate (s^{-1})
k_f	receptor/ligand association rate (cm^2/s)
k_r	receptor/ligand complex dissociation rate (s^{-1})
k_{ro}	intrinsic receptor/ligand complex dissociation rate in absence of stress (s^{-1})
K_d	equilibrium receptor/ligand dissociation constant (cm^{-2})
L	cell length (cm)
n	adhesion receptor number density ($molecules/cm^2$)
n_s	substratum ligand density ($molecules/cm^2$)
N	dimensionless adhesion receptor number density, Eq. A2
R	adhesion receptor number (#)
t	time (min)
T	temperature (K)
u	node displacement (cm)
v	cell speed (cm/s)
W	cell width (cm) or contractile energy per bond (erg/bond)
x	distance along length of cell (cm)
X	dimensionless distance along length of cell, Eq. A1
y	distance across width of cell (cm)
Y	dimensionless distance across width of cell, Eq. A1

Subscripts

b	bound receptor
body	cell body
c	contraction, cytoskeletal, or cytoskeleton-bond connection
end	pseudopodal element not connected to bonds
i	node or compartment number
l	lamellipodal extension or lamellipodal
m	movement cycle
max	maximal
r	relaxation or free receptor
spring	bond
T	total
u	uropodal

Superscripts

d	dorsal
v	ventral

Greek letters

α	dimensionless cell stiffness, Eq. A13a
β	ratio of contraction time to movement cycle time, Eq. A17
γ	ratio of total pseudopodal stiffness to cell body stiffness, Eqs. A15a, b
δ	cell aspect ratio, Eq. A3
ϵ	strenth of connection between bond and cytoskeleton, Eq. A13c
η	dimensionless receptor diffusivity, Eq. A3
κ	dimensionless cell-substratum adhesiveness, Eq. 16
λ	fraction of leading edge of cell for receptor insertion
ν	dimensionless cell speed, Eq. A4
θ	dimensionless endocytosis rate, Eq. A3
ρ	ratio of total ventral receptors in lamellipod to total ventral receptors in uropod, Eq. A22
σ	intrinsic pseudopodal stiffness in absence of bonds, Eq. A13d
τ	dimensionless time, $k_{ro}t$
μ	cell viscosity (dyn-s/cm^2)
$\bar{\omega}$	ratio of dimensionless cell viscosity to dimensionless cell stiffness, Eq. 24
ω	dimensionless cell viscosity, Eq. A13b
ψ	ratio of intrinsic dissociation rates in absence of stress between lamellipod and uropod, Eq. 12
ζ	dimensionless node displacement, Eq. A12

MATHEMATICAL MODEL

Observed under a microscope, the movement of an individual tissue cell appears roughly as a jerky sequence of spreading at the periphery, most pronounced at the front of the cell, followed by net movement of the main body of the cell and retraction of the cell's tail (Trinkaus, 1976; Lackie, 1986). Unidirectional cell movement can, then, be viewed as a sequence of three distinct stages (Fig. 1). During the first stage of this cycle, a period t_l, the cell extends a thin sheet of cytoplasm and membrane, known as a lamellipod, in the forward direction of motion. Because we are concerned here only with one-dimensional movement, we will not be interested in any angular direction in which the lamellipod might extend. Allowing changes in angular direction would be important to analyze for the effects of cell bias, either by chemotaxis or possibly haptotaxis (Carter, 1965), on movement. Also, we will ignore in our present approach detailed descriptions of what signals the cell to extend a pseudopod or the biophysics of this extension (for work on this process see Dembo et al., 1984; Oster and Perelson, 1987; and Zhu and Skalak, 1988). Here we will be concerned with only the duration of lamellipod extension. As the lamellipod extends, adhesion receptors on the ventral side of the extension will form bonds with ligand on the underlying substratum. We assume

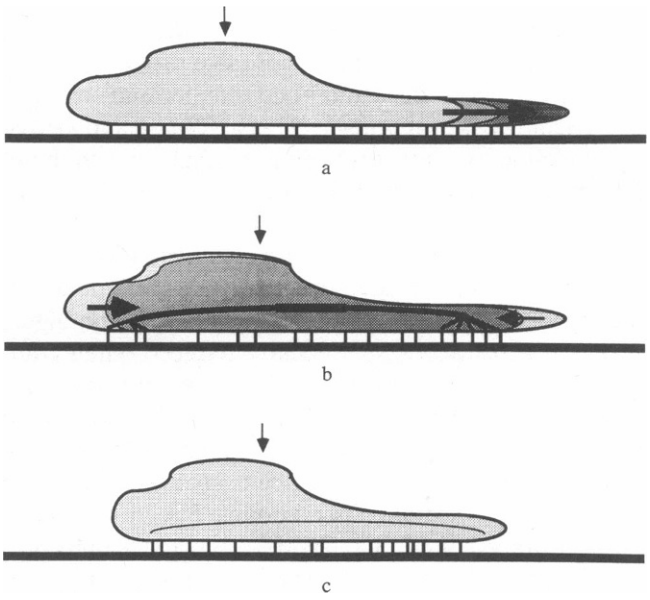

FIGURE 1 Illustration of chronological cycle of events in movement of a tissue cell over an adhesive substratum. (*a*) In first stage of cycle, cell extends lamellipod in direction of movement. Adhesion receptors bind reversibly with ligand attached to the underlying substratum. (*b*) Cytoskeleton of cell contracts during second part of cycle. The force generated by intracellular contractile events is transmitted to the surface through adhesion bonds. If an asymmetric distribution of bonds is present, the traction force exerted is also asymmetric and the cell experiences net displacement in the direction of movement. (*c*) In the last stage of the cycle the cytoskeleton relaxes, and a new adhesion bond distribution is reached. The cell now repeats the cycle. The arrows here depict the location of the cell's center of mass at each point in the cycle. Note that the center of mass moves greatest during the contractile stage (*b*).

that by the end of this process, all receptor/ligand interactions reach a state of equilibrium.

During the second stage of the movement cycle, a period of duration t_c, the cell's actin-based cortical cytoskeleton contracts (Heath, 1983), pulling on both ends of the cell body (Trinkaus, 1984). Because some of the elements of the cytoskeleton are connected to the adhesion bonds, the cytoskeleton pulls at the bonds at either end of the cell, resulting in the breakage of some bonds at the lamellipod and uropod (the cell posterior). Although the cell is attached to the surface underneath its entire length, we will assume that the attachments at either end are most important in locomotion (Chen, 1981). If asymmetry exists in the number of cell/substratum bonds between the lamellipod and uropod, arising from a number of plausible mechanisms involving receptor trafficking or dynamics, a net traction force on the substratum will be generated. Translocation of the cell mass opposing this traction force will occur if the substratum is fixed. When it is not fixed, the substratum itself will be deformed, as demonstrated experimentally (Harris et al., 1980). The actual force transmitted to the bonds after cell deformation, as well as the net resulting traction force, will depend on adhesive properties, such as adhesion-receptor/ligand bond number and strength, and rheological properties, such as stiffness and viscosity. Mechanisms for producing cell/substratum bond number asymmetry will be considered shortly.

Recent work by Marks et al. (1991) appears to support our conceptual view of the separate contributions of the lamellipodal and uropodal regions to migration. Movement speed of polymorphonuclear leukocytes on highly adhesive substrata is significantly reduced when transient increases in intracellular Ca^{2+} concentrations are prevented. This reduction appears to result from an inability of the cells to detach their uropods from the substratum in the absence of such transients rather than an inability to extend lamellipodia. Speed is further reduced when competing ligand for the adhesion receptors is added in solution, now due to an inability of extended lamellipodia to attach to the substratum.

Finally, during the third stage of the cycle lasting a period t_r, the cytoskeleton relaxes as the contractile apparatus no longer transmits force to the bonds, and adhesion receptors are free to reach unstressed distributions. The entire cycle thus has a length

$$t_m = t_l + t_c + t_r. \quad (1)$$

Two mechanisms for generating spatial asymmetry in adhesion bond number between the lamellipod and uropod appear especially attractive at present. Endocytosis of unbound adhesion receptor over the entire cell surface and preferential insertion at the lamellipod could result in the accumulation of receptors at the front of the cell (Bretscher, 1989). Constitutive endocytosis of the fibronectin receptor (FnR) has been shown in CHO cells using monoclonal antibodies against either the β subunit (Raub and Kuentzel, 1989) or the intact receptor (Sczekan and Juliano, 1990), while the presence of FnR within the cytoplasm of motile cells, detected using immunoflouresence, has been interpreted as evidence for internalization (Duband et al., 1988*a*). Further, some recent experiments suggest that endocytosed FnR may be recycled preferentially to the cell's leading edge (Bretscher, 1989). Alternatively, adhesion-bond number asymmetry will occur if a spatial variation in receptor/ligand affinity exists between the lamellipod and uropod. Localized proteolysis of adhesion receptor at the uropod (Grinnell, 1986) has been suggested, while Gailit and Ruoslahti (1988) have shown that the replacement of Ca^{2+} with Mn^{2+} can increase receptor/ligand affinity. Further, integrins can be phosphorylated (Hirst et al., 1986), with receptor phosphorylation reducing the Fn binding activity of FnR (Tapley et al., 1989). Thus, several mechanisms could plausibly establish a locally selective modulation required for enhanced receptor/ligand affinity at the lamellipod relative to the uropod.

The events of lamellipodal extension, cytoskeletal contraction, and subsequent relaxation can be put into a quantitative framework using two complementary approaches. Adhesion receptor dynamics and trafficking can be described as a reaction-diffusion problem for receptors interacting with immobilized ligand. A viscoelastic-solid model can be used to describe both how the force generated by cytoskeletal elements is transmitted to the adhesion bonds at either end of the cell and how this force affects both bond dynamics and the net deformation of the cell. Because the amount of force transmitted to each end of the cell will depend not only on the particular rheological properties and deformation of the cell under stress but also on the adhesion bond distribution, the two models are coupled. Mathematically, the receptor distribution model will describe events during the entire cycle whereas the viscoelastic model will only describe events during the contraction phase of cycle. Then, the net speed of translocation determined from cell displacement during the contraction phase can be averaged over the entire movement cycle to obtain an observable movement speed.

Receptor dynamics model

To easily determine the distribution of adhesion receptors on a moving cell, it is necessary to approximate the cell's geometry. Because we only are concerned spatially with surface trafficking events, we can treat the cell surface as two sheets sewn together along all edges (Fig. 2).

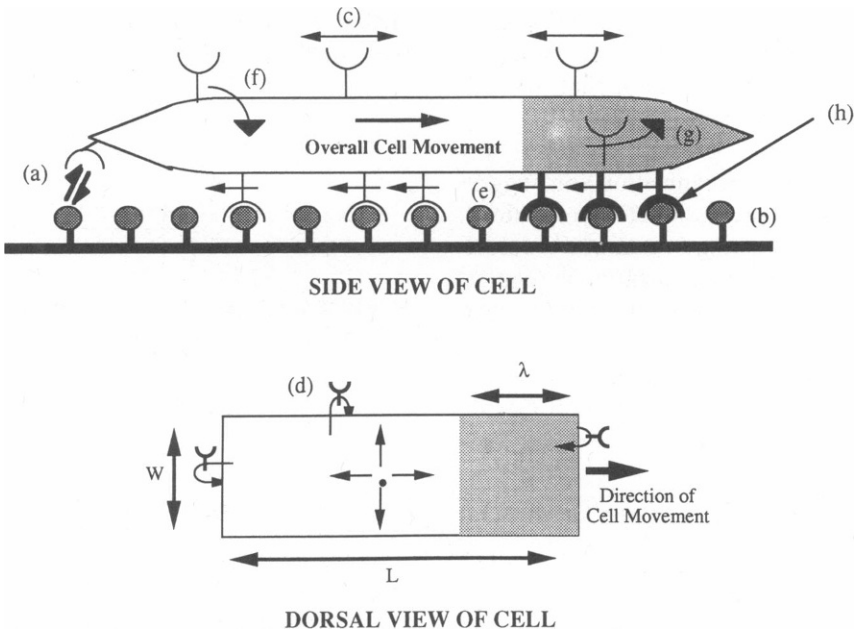

FIGURE 2 Schematic diagram of adhesion-receptor trafficking events during cell migration over adhesive substrata. The cell surface is modeled as two flat rectangular sheets, representing the dorsal and ventral faces, sewn together along their edges to form a continuous surface. Receptors on the ventral surface bind reversibly with adhesive ligand (*a*), immobilized on the substratum at a uniform density (*b*). Free adhesion receptors can diffuse on either surface (*c*) and can also diffuse between the dorsal and ventral faces (*d*). Bound receptors drift backwards with respect to the cell at the cell's forward velocity (*e*). Two mechanisms for generating an asymmetric adhesion bond distribution are illustrated: free receptors can be endocytosed (*f*) and preferentially inserted over the leading λ of the cell (*g*), or receptors at the front of the cell may bind more tightly to ligand than those at the rear (*h*).

This rectangular model has been used by Dembo et al. (1981) and allows calculations without specification of complicated cell shapes. We neglect curvature effects and treat each sheet as a flat two-dimensional surface, so that any position on either sheet can be described by the two coordinates x and y, where x is the distance from the posterior edge of the cell and y is the distance perpendicular to the cell's centerline. Each sheet has length L and width W. The top (dorsal) sheet contains only free receptors, whereas the bottom (ventral) has both free receptors and receptors bound to ligand immobilized on the underlying substratum. The distribution of adhesion receptors on the two faces of the cell surface depends on the parameters describing binding and trafficking events. Denote the density of free receptors on the dorsal and ventral surfaces as n_r^d and n_r^v, respectively, and let n_b be the density of bound receptors on the ventral surface. The total number of adhesion receptors on the surface is R_T:

$$\int_0^L \int_{-W/2}^{W/2} (n_r^d + n_r^v + n_b)\, dy\, dx = R_T. \qquad (2)$$

We assume that the primary force in adhesion is due to specific and reversible interactions between receptors and neglect any nonspecific interactions (see Bongrand and Bell, 1984). Then, free receptors on the ventral surface can bind reversibly with ligand on the underlying substratum. Bonds form at a rate k_f and dissociate at an intrinsic rate k_{ro}. We also assume here that the ligand is present in excess at a uniform concentration of n_s, so that we can treat this density as a constant.

Free receptors on the dorsal and ventral surfaces diffuse at a rate D_r. Because the dorsal and ventral surfaces are joined at all edges and receptors must be conserved, free receptors nearing the edge of the cell on one surface can diffuse over the edge onto the other surface. Further, free receptors may be internalized by endocytosis into the cell's interior at a rate k_e. Assuming the total number of adhesion receptors R_T is at steady state, the rates of insertion of receptors into the cell surface and internalization must be equal. Because our model will only be applicable to persistent, stable cell migration, we assume that the cell is directionally polarized and that fresh receptors are replenished on both faces of the cell's surface over a fraction λ of the cell length from the leading edge, at a rate which balances internalization. These fresh receptors will be equally distributed between the two faces of the cell over this forward region. Finally, because we choose our frame of reference to be the cell body, bound receptor/

ligand complexes will appear to "convect" backwards relative to the cell's center of mass at the cell's overall forward velocity of v. It should be noted that no bulk membrane flow is assumed to occur.

A feature neglected in this present model is any functional effects of receptor organization into aggregates, such as focal contacts, by cytoskeletal interactions. Though it would be very interesting to examine theoretically the possible role of receptor organization in regulating cell migration, there is currently little quantitative information bearing on this phenomenon.

Mass balances for free receptor on the dorsal and ventral surfaces in the forward λL of the cell can be written as:

$$\frac{\partial n_r^d}{\partial t} = D_r \nabla^2 n_r^d - k_e n_r^d + \frac{k_e}{2\lambda L W} \int_0^L \int_{-W/2}^{W/2} (n_r^d + n_r^v)\, dy\, dx \quad (3a)$$

$$\frac{\partial n_r^v}{\partial t} = D_r \nabla^2 n_r^v - k_f n_s n_r^v + k_{ro} n_b - k_e n_r^v + \frac{k_e}{2\lambda L W} \int_0^L \int_{-W/2}^{W/2} (n_r^d + n_r^v)\, dy\, dx. \quad (4a)$$

In the rear $(1 - \lambda)L$ of the cell the equivalent balances are:

$$\frac{\partial n_r^d}{\partial t} = D_r \nabla^2 n_r^d - k_e n_r^d \quad (3b)$$

$$\frac{\partial n_r^v}{\partial t} = D_r \nabla^2 n_r^v - k_f n_s n_r^v + k_{ro} n_b - k_e n_r^v. \quad (4b)$$

Over the entire ventral (underlying) surface, the balance on bound receptors is:

$$\frac{\partial n_b}{\partial t} = k_f n_s n_r^v - k_{ro} n_b + v \frac{\partial n_b}{\partial x}. \quad (5)$$

To solve Eq. 3–5 at steady state nine boundary conditions are needed: four for each free receptor distribution and one for the distribution of bound receptors. Free receptor continuity along the "seams" of surfaces provides four boundary conditions:

$$n_r^d\left(x, y = \frac{W}{2}\right) = n_r^v\left(x, y = \frac{W}{2}\right) \quad (6a)$$

$$n_r^d\left(x, y = \frac{-W}{2}\right) = n_r^v\left(x, y = \frac{-W}{2}\right) \quad (6b)$$

$$n_r^d(x = 0, y) = n_r^v(x = 0, y) \quad (6c)$$

$$n_r^d(x = L, y) = n_r^v(x = L, y). \quad (6d)$$

The four remaining boundary conditions arise because no net receptor flux can occur at the sides of the cell. Along the sides of the cell, the flux equations include only the free receptors:

$$-D_r \left.\frac{\partial (n_r^d + n_r^v)}{\partial y}\right|_{x,y=W/2} = 0 \quad (6e)$$

$$-D_r \left.\frac{\partial (n_r^d + n_r^v)}{\partial y}\right|_{x,y=-W/2} = 0, \quad (6f)$$

whereas the flux expressions for the front and rear of the cell include terms for bound receptor "convection."

$$-D_r \left.\frac{\partial (n_r^d + n_r^v)}{\partial x} + v n_b\right|_{x=0,y} = 0 \quad (6g)$$

$$-D_r \left.\frac{\partial (n_r^d + n_r^v)}{\partial x} - v n_b\right|_{x=L,y} = 0. \quad (6h)$$

We emphasize that this convection is due to frame of reference effects and not bulk membrane lipid flow. Conservation of receptors (Eq. 2) provides the final boundary condition.

Cell mechanics model

The remaining requirement for persistent cell migration is intracellular force generation. Although in recent years many details of cytoskeletal function have been identified, many of the mechanisms involved in force generation and transmission have yet to be definitively elucidated. Rather than develop a model for how cells generate force which depends on assumptions for detailed molecular events, we can represent cytoskeletal dynamics at a conceptual level using a viscoelastic-solid model. Viscoelastic-solid models are appropriate for modeling the deformation of cells, which possess properties of both fluidity and stiffness (Dong et al., 1988). Fluidity can be modeled by linear viscous dashpots, in which stress is proportional to the rate of strain, with viscosity as the proportionality constant. Likewise, cell stiffness can be represented with linear elastic springs: stress is proportional to strain by a Hookean spring constant.

A schematic of our viscoelastic-solid representation of a tissue cell is presented in Fig. 3 *a*. The cell is divided into six compartments, each of length $L/6$. The inner four compartments are identical and consist of a spring, dashpot, and contractile element in parallel. These compartments describe the mechanics of the cell body. The outer compartments, representing the uropod and lamellipod, also consist of dashpots and springs in parallel, but in these compartments we include two types of springs: a spring for the intrinsic stiffness of each

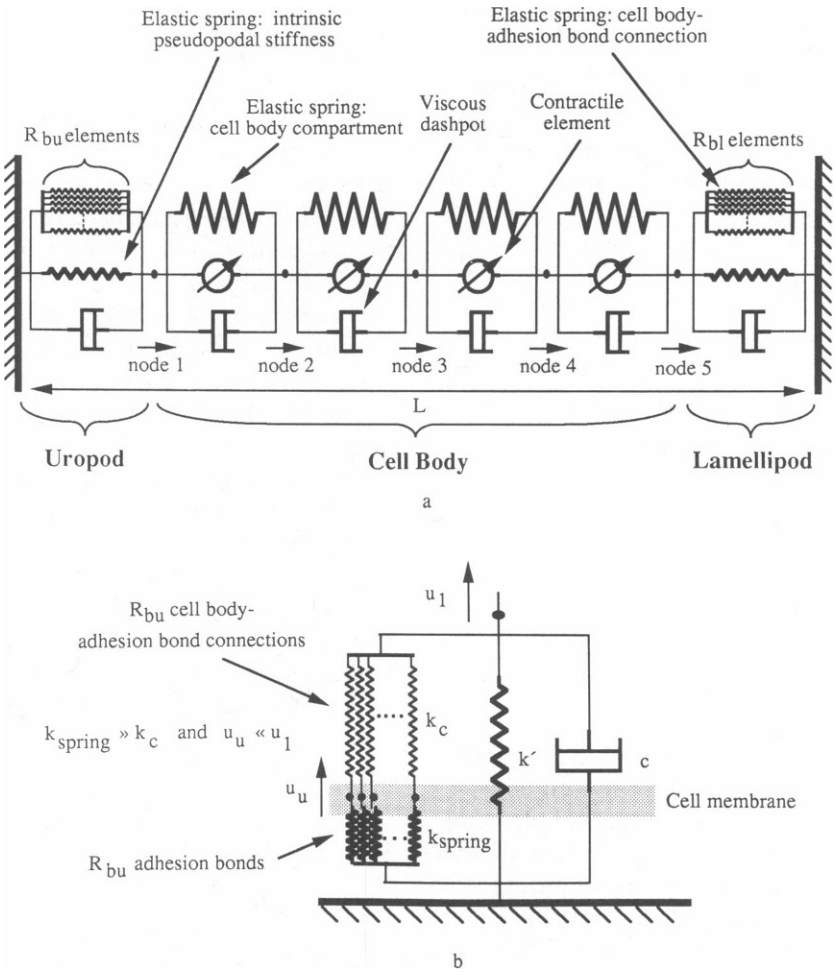

FIGURE 3 Illustration of viscoelastic-solid model describing cell mechanics during locomotion. (*a*) The cell can be divided into six compartments. The middle four compartments, representing the cell body, contain identical Hookean springs and viscous dashpots in parallel with a contractile element, whereas the leading (lamellipodal) and trailing (uropodal) compartments possess similar springs and dashpots. These latter elements are in parallel with R_{bl} and R_{bu} springs describing the connection between cell body and adhesion bonds in the lamellipod and uropod, respectively. The compartments are separated by nodes, whose displacement determines the deformation and translocation of the cell. (*b*) Detailed picture of arrangement of viscoelastic elements in the uropodal compartment. A Hookean spring and dashpot describe the intrinsic stiffness and viscosity of the pseudopod in the absence of adhesion bonds. In parallel, each adhesion bond in this compartment is treated as a spring in series with a spring representing the cytoskeletal-adhesion bond connection. Assuming that each adhesion bond is stiffer than its cytoskeletal connection, the displacement u_u is much less than $(u_1 - u_u)$, and the effects of u_u and k_{spring} can be neglected explicitly in formulating node displacement balances. The lamellipod is described by an identical arrangement.

pseudopod and springs representing connections between the cell body and adhesion bonds. These latter springs transmit the cell-body generated contractile force to the adhesion bonds and the underlying substratum to provide the net traction necessary for movement in the presence of bond asymmetry. Neglecting the effects of organelles, such as the nucleus, and allowing the cell to deform only one-dimensionally, we can assume that the mechanical properties of each compartment are homogeneous. The arrangement of viscoelastic elements in each compartment is essentially a limiting case of the standard viscoelastic-solid model used by Schmid-Schonbein et al. (1981) obtained by deleting an additional elastic element in series with the viscous element. This deletion is reasonable because for tissue cells the events of contraction will occur over comparatively long time scales. Although Evans and Yeung (1989) found that an anisotropic Maxwell fluid surrounded by a cortical shell better describes the long-time scale deformation of granulocytes, the deformation of adherent tissue cells additionally is limited due to cytoskeleton/adhesion bond/substratum linkages. This

additional resistance can be described appropriately by the parallel elastic element.

While the boundaries at either end of cell are stationary, each compartment is connected to its adjacent compartments by a node. The displacement of each node u_i between adjacent compartments can be found by balancing the forces acting on it:

$$\text{Node } x_1\text{:}\quad c\frac{du_1}{dt} + k'u_1 + k_u u_1 = c\frac{d(u_2-u_1)}{dt} + k(u_2-u_1) + F_2 \quad (7a)$$

$$\text{Nodes } x_2 - x_4\text{:}\quad c\frac{d(u_i-u_{i-1})}{dt} + k(u_i-u_{i-1}) + F_i = c\frac{d(u_{i+1}-u_i)}{dt} + k(u_{i+1}-u_i) + F_{i+1} \quad i = 2, 3, 4 \quad (7b)$$

$$\text{Node } x_5\text{:}\quad c\frac{d(u_5-u_4)}{dt} + k(u_5-u_4) + F_5 = c\frac{d(-u_5)}{dt} + k'(-u_5) + k_l(-u_5). \quad (7c)$$

The parameter c describes the viscosity of the dashpots, k the stiffness of each compartment in the cell body, k_u the stiffness of the uropod due to cytoskeletal elements connected to adhesion bonds, k_l the stiffness of the lamellipod due to cytoskeletal elements connected to adhesion bonds, k' the intrinsic stiffness of the pseudopods in the absence of adhesion bonds, and F_i the force generated in compartment i.

The frame of reference of each node is the origin, so that at the start of contraction $t = 0$:

$$u_i(t = 0) = 0 \quad i = 1, \ldots, 5, \quad (8)$$

whereas each node also is constrained to remain within the cell body:

$$-\frac{iL}{6} \le u_i(t) \le \frac{(6-i)L}{6} \quad i = 1, \ldots, 5. \quad (9)$$

Contraction lasts for a period t_c.

Both the uropodal and lamellipodal compartments contain elements connecting the main body of the cell to adhesion bonds. The simplest way to represent these pseudopodal elements is to assume that the stiffness of each element is proportional to the number of adhesion bonds present in each compartment:

$$k_u = k_c R_{bu} \quad (10a)$$

$$k_l = k_c R_{bl}, \quad (10b)$$

where k_c is the stiffness contributed by cytoskeletal connection to one adhesion bond and R_{bu} and R_{bl} are the number of adhesion bonds in the uropod and lamellipod, respectively. We can treat the adhesion bonds themselves as springs (Dembo et al., 1988) (see Fig. 3 *b*). If we assume that the spring constant for a bond, k_{spring}, is much greater than the spring constant for the cytoskeletal element linking the bond to the cell body, k_c, the bond displacements u_u and u_l will be much less than the cytoskeletal displacements u_1 and u_5, respectively. Then, we can neglect these bond displacements to estimate u_1 and u_5 directly.

The number of adhesion bonds in the uropod and lamellipod can be described using simple kinetic expressions. Here we treat each of these compartments as homogeneous for free and bound receptors and allow the bonds to be uniformly stressed by the cytoskeleton. If the kinetics of receptor-ligand association/dissociation are much faster than the kinetics of cell deformation, as will be the case here, the bonds will be in pseudo-steady state during contraction (Lauffenburger, 1989). Once again, we neglect depletion of ligand. We can then write balances on the number of bonds in the uropod and lamellipod R_{bu} and R_{bl}, respectively, as a function of free receptors in each compartment (R_{ru} and R_{rl}) as

$$\frac{dR_{bu}}{dt} = k_f n_s R_{ru} - k_{ru} R_{bu} = 0 \quad (11a)$$

$$\frac{dR_{bl}}{dt} = k_f n_s R_{rl} - k_{rl} R_{bl} = 0. \quad (11b)$$

We assume, as originally suggested by Bell (1978), that the forward rate constant k_f is independent of the force applied to bonds but the reverse rate constants k_{ru} and k_{rl} depend on the forces applied to bonds in the uropod and lamellipod, respectively. We also adopt his expression for the role of force in the dissociation rate of a bond: the dissociation rate is the product of an intrinsic dissociation rate in the absence of stress, k_{ro}, and an exponential of contractile energy per bond divided by thermal energy. This treatment is based on an analysis by Zhurkov (1965) for the effects of stress on material fracture. To allow the bonds in the rear of the cell to have a higher intrinsic dissociation rate than bonds in the front, as might happen in the presence of selectively secreted proteases at the uropod or Mn^{2+} at the lamellipod, we introduce ψ as the ratio of intrinsic dissociation rates in the absence of stress between front and back:

$$\psi = \frac{k_{rl}\{F_{bl} = 0\}}{k_{ru}\{F_{bu} = 0\}} \quad (12)$$

Allowing ψ to deviate from unity provides one mechanism for inducing receptor/ligand bond asymmetry across the cell's length.

The rates of dissociation, then, are functions of the contractile energies per bond, W_u and W_l, input to the

bonds by the cytoskeleton to stretch the bonds a distance u_u or $-u_l$:

$$k_{ru} = \frac{k_{ro}}{\Psi} e^{(W_u/k_bT)} = \frac{k_{ro}}{\Psi} e^{(F_{bu}u_u/R_{bu}k_bT)} \tag{13a}$$

$$k_{rl} = k_{ro}\, e^{(W_l/k_bT)} = k_{ro} e^{(F_{bl}u_l/R_{bl}k_bT)}. \tag{13b}$$

These forces F_{bu} and F_{bl} can be related to the spring constant for the connecting cytoskeleton k_c, the bond spring constant k_{spring}, the number of bonds (R_{bu} or R_{bl}), and the displacements of the bonds (u_u and $-u_l$) and cytoskeletal elements (u_l and $-u_5$):

$$F_{bu} = k_c R_{bu} u_l = k_{spring} R_{bu} u_u \tag{14a}$$

$$F_{bl} = k_c R_{bl}(-u_5) = k_{spring} R_{bl}(-u_l). \tag{14b}$$

Substituting Eqs. 12–14 into Eq. 11 and rearranging, the total number of bonds in each compartment is:

$$R_{bu}\{u_l\} = \frac{R_{Tu}}{1 + \Psi\kappa^{-1} \exp\left(\dfrac{k_c^2 u_l^2}{k_{spring} k_b T}\right)} \tag{15a}$$

$$R_{bl}\{u_5\} = \frac{R_{Tl}}{1 + \kappa^{-1} \exp\left(\dfrac{k_c^2 u_5^2}{k_{spring} k_b T}\right)}. \tag{15b}$$

The dimensionless receptor/ligand bond affinity (cell-substratum adhesiveness) κ, defined as

$$\kappa = \frac{k_f n_s}{k_{ro}} = \frac{n_s}{K_d} \tag{16}$$

is directly proportional to the surface ligand density and inversely proportional to the receptor/ligand equilibrium dissociation constant K_d, which provides a measure of the strength of receptor/ligand association. Note that the effective affinity of the uropod is decreased by a factor of ψ compared with the lamellipod. The total number of adhesion receptors on the ventral sides of the uropod and lamellipod are

$$R_{Tu} = \int_{5L/6}^{L} \int_{-W/2}^{W/2} (n_r^v + n_b)\, dydx \tag{17a}$$

$$R_{Tl} = \int_{0}^{L/6} \int_{-W/2}^{W/2} (n_r^v + n_b)\, dydx. \tag{17b}$$

Combinining these expressions for bond number with the force balances, Eq. 7 can be rearranged as a nonlinear first-order matrix differential equation:

$$\frac{du}{dt} = A\{u\}u + BF \tag{18a}$$

where

$$A\{u\} = \ldots \tag{18b}$$

$$B = \ldots \tag{18c}$$

$$u = \begin{bmatrix} u_1 \\ u_2 \\ u_3 \\ u_4 \\ u_5 \end{bmatrix} \quad F = \begin{bmatrix} F_1 \\ F_2 \\ F_3 \\ F_4 \\ F_5 \end{bmatrix} \tag{18d}$$

The cell's overall velocity can then be given as the average velocity of each of these nodes over a full movement cycle of extension, contraction, and relaxation:

$$v = \frac{\sum_{i=1}^{5} u_i(t = t_c)}{5t_m}. \tag{17}$$

Model analysis and solution

Details of equation scaling and model solution procedure are presented in the Appendix. Eq. 16 and 12, respectively, define dimensionless cell-substratum adhesiveness κ and the ratio of uropodal to lamellipodal adhesiveness ψ. Dimensionless rates of endocytosis θ and adhesion receptor diffusion η can be found by scaling the relevant dimensional parameters to the key time scale k_{ro}, the intrinsic adhesion bond dissociation rate. δ is the cell aspect ratio. Cross-sectional areas can be used to relate each Hookean spring constant to a Young's modulus E and the dashpot coefficient to viscosity μ. Contractile force, cell stiffness, and cell viscosity can in turn be dedimensionalized with respect to the spring force $\sqrt{k_{spring} k_b T}$ as f_c, α, and ω, respectively. In this present work we assume that each cell body compartment generates a uniform force in both time and space. This assumption can be relaxed, of course, to more general force conditions when interest warrants.

Other key dimensionless parameters include ϵ, a measure of strength of connection between an adhesion bond and cytoskeleton, and σ, the ratio of intrinsic pseudopodal stiffness in the absence of adhesion bonds to cell body stiffness. Larger values of ϵ correspond to a greater input of contractile energy to the bonds. Finally, dimensionless contraction time τ_c is the product of dimensional contraction time and the key time scale k_{ro}, and the fraction of movement cycle time spent in contraction is β.

Ranges for these key dimensionless parameters in our model appropriate for tissue cells, such as fibroblasts and endothelial cells, are presented in Table 1. These estimates are based on reported literature values and experimental observations. With the pseudo-steady-state assumption that receptor/ligand kinetics are faster than cytoskeletal contraction dynamics and, neglecting bound receptor convection with respect to the cell as a

TABLE 1 **Estimated ranges of dimensionless parameters**

Paramater	Definition	Range
κ	Cell-substratum adhesiveness	10^{-3}–10^{3}
θ	Endocytosis rate	10^{-6}–1
δ	Cell aspect ratio	1–20
η	Receptor diffusivity	10^{-8}–10^{-2}
λ	Fraction of leading edge receptor insertion takes place	0.1–0.5
Ψ	Ratio of uropodal to lamellipod adhesiveness	10^{-4}–1
f_c	Force generated per compartment	10^{0}–10^{6}
α	Stiffness	10^{-1}–10^{5}
ω	Viscosity	10^{1}–10^{7}
ϵ	Strength of adhesion bond/cytoskeleton attachments	10^{-4}–10^{-1}
σ	Ration of pseudopodal stiffness in the absence of bonds to cell body stiffness	10^{-3}–1
τ_c	Contraction time	10^{-1}–10^{5}
β	Fraction of movement cycle for contraction	0.1–0.5

(See Table A1 for estimates of underlying dimensional parameters.)

frame of reference, the equations describing receptor trafficking are independent of the viscoelastic-solid model. Then, dimensionless cell speed v, scaled with k_{ro} and cell length L, can be found by integrating the dimensionless node displacement matrix equation. This approach is valid for large adhesion bond asymmetries.

RESULTS AND DISCUSSION

Model predictions

Computational results are shown in terms of dimensionless cell speed, v, equal to the measurable dimensional speed v divided by the product $k_{ro}L$, which is basically the velocity of adhesion bond dissociation in the absence of mechanical stress. Hence, the true, dimensional speed v can be calculated easily by multiplying plotted scaled speed v by $k_{ro}L$. For example, if $L = 25$ μm and $k_{ro} = 40$ min^{-1} (from $K_d = 10^{-7}$ M and $k_f \approx 4 \cdot 10^8$ M^{-1} min^{-1}), then $k_{ro}L = 10^3$ μm/min. Typical maximum dimensionless speed on the figures to follow is on the order $v \sim 10^{-3}$, yielding a true dimensional speed of roughly 60 μm/h. Clearly, then, the model can predict cell speeds which are reasonable for tissue cell migration.

Our prediction of central interest is the dependence of cell speed on cell-substratum adhesiveness, κ. κ is the product of ligand density and adhesion-receptor/ligand affinity, $\kappa = n_s/K_d$. The effect of κ on cell speed for asymmetry generated by differential bond affinity, in which the uropodal bond affinity is less than the lamellipodal bond affinity (i.e., $\psi < 1$ from Eq. 12), is plotted in Fig. 4. Here, the possibility of polarized endocytic trafficking is omitted ($\theta = 0$). When no difference in adhesiveness exists between the front and rear of the cell ($\psi = 1$), no movement occurs because no asymmetry has been created. Decreasing adhesiveness at the rear (or increasing adhesiveness at the front) by decreasing ψ results in a biphasic relationship between movement speed and adhesiveness because bond-number asymmetry has been created. At low adhesivity κ, cytoskeletal contraction dissociates the few receptors that have bound at both lamellipod and uropod, so no net movement occurs. Increasing adhesivity results in the formation of more bonds at both ends of the cell; however, the lamellipod will have more bonds than the uropod because of greater relative affinity at the cell front. During contraction the posterior cell regions are displaced more than the anterior regions because there are fewer posterior bonds to withstand the contractile force, and the cell experiences a net forward translocation. With further increases in adhesivity more receptors will be present in the uropod and additional bonds will form there until enough bonds exist to withstand the contractile force without completely dissociating. Net translocation of the cell will then decrease. The region of

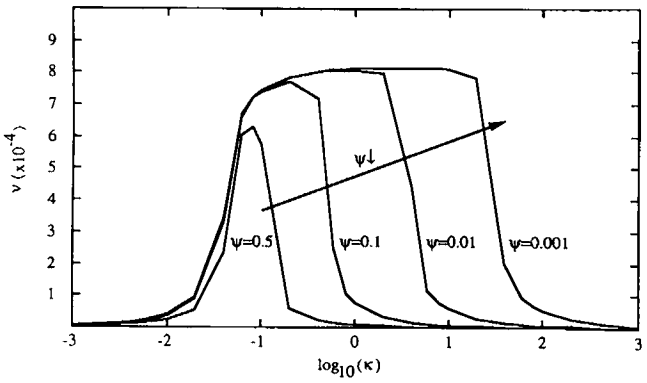

FIGURE 4 A biphasic relationship between dimensionless cell-substratum adhesiveness κ and dimensionless cell speed v can arise when bond distribution asymmetry results from a spatial variation in strength of adhesion-receptor/ligand binding. ψ is the ratio of uropodal to lamellipodal adhesiveness. Values of ψ near unity correspond to small differences in bond affinity between front and rear of the cell, and the cell moves at nontrivial speeds over a restricted range of adhesiveness. Decreasing ψ leads to the generation of greater adhesion-bond asymmetry, and cell movement can occur over a larger range of adhesiveness. Note that the maximum rate of migration does not depend significantly on ψ. $\theta = 0$, $R_T = 6 \cdot 10^5$, $\eta = 10^{-5}$, $\delta = 10$, $\lambda = 0.333$, $f_c = 2 \cdot 10^3$, $\alpha = 300$, $\omega = 100$, $\epsilon = 2 \cdot 10^{-3}$, $\sigma = 0.5$, $\tau_c = 180$, and $\beta = 0.5$.

adhesiveness permitting substantial cell migration is strongly affected by the affinity asymmetry ψ, ranging from only a single order of magnitude in κ to a few decades in κ as ψ decreases. Note that cell speed always diminishes to zero at sufficiently large adhesiveness because enough uropodal bonds can be maintained under contraction to resist cell displacement.

An analogous plot, for the alternative case in which bond-number asymmetry results from polarized receptor recycling ($\theta > 0$), with bond affinity now constant along the cell ($\psi = 1$), is shown in Fig. 5. Again, cell speed can exhibit a biphasic dependence on cell-substratum adhesiveness, although for large values of θ (high rates of endocytosis), monophasic behavior develops. Increasing θ corresponds to increasing adhesion-receptor number asymmetry between the lamellipod and the uropod. Thus, for the case of polarized receptor trafficking, θ plays much the same role as ψ for a spatial variation in bond affinity. At sufficiently great θ, the uropod will not have enough total receptors to be able to form enough bonds to resist displacement at any level of adhesiveness, so that cell speed will not decrease with increasing adhesiveness. At lower θ enough receptors will be present in the rear of the cell to form the necessary bonds to resist contraction and prevent movement.

These two asymmetry mechanisms predict distinct behavior for the effect of adhesion-receptor number, R_T, on the relationship between speed and cell-substratum adhesiveness. Fig. 6 compares these predictions. For the case of differential bond affinity decreasing R_T serves merely to shift the speed vs. adhesiveness curve to higher values of κ. In contrast, for the case of polarized receptor recycling decreasing R_T transforms the cell speed curve from a biphasic to a monophasic dependence on adhesiveness. Increasing adhesion bond asymmetry through decreases in ψ or increases in θ allows significant movement over a broader range of adhesiveness. However, for the differential bond affinity mecha-

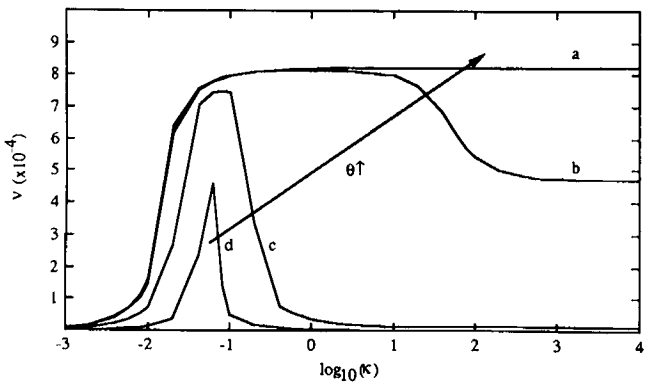

FIGURE 5 Model calculations for the effect of dimensionless cell-substratum adhesiveness κ on dimensionless movement speed v at different dimensionless receptor internalization rates θ for generation of adhesion bond asymmetry through endocytosis and preferential receptor insertion. At sufficiently low θ (and recycling, corresponding to small asymmetries in total receptor number between the lamellipod and uropod, $R_{T\ell}$ and R_{Tu}, respectively), speed shows a biphasic dependence on adhesiveness: at low κ, not enough adhesion bonds form at the front of the cell to resist contraction, whereas at high κ formation of bonds at the cell's rear retards movement. However, at higher θ, dimensionless movement speed does not decrease significantly as adhesiveness is increased because at the uropod too few receptors are present to produce sufficient bond number to withstand contraction even on highly adhesive substrata. Note that maximum cell speed is independent of receptor number. Parameter values are the same as presented in Fig. 4 except $\psi = 1$ and θ is varied: (*a*) 10^{-1} and 10^{-2}; (*b*) 10^{-3}; (*c*) 10^{-4}; (*d*) 10^{-5}.

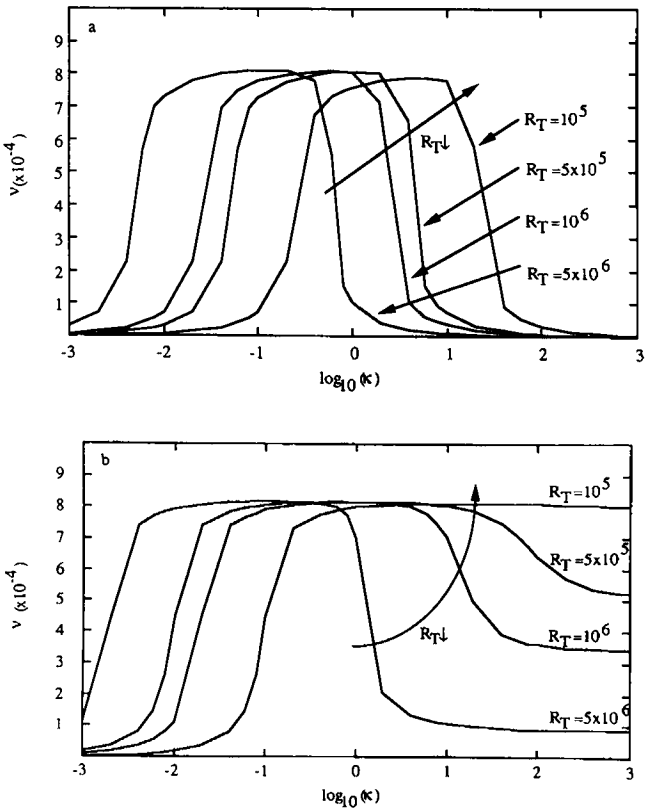

FIGURE 6 Comparison of two alternative bond distribution asymmetry mechanisms in terms of the influence of adhesion receptor number R_T. (*a*) For the differential bond affinity mechanism, the dependence of cell speed on substratum adhesiveness is always biphasic regardless of R_T. The range of adhesiveness permitting substantial migration speed is also independent of R_T. Parameter values are the same as in Fig. 4 except $\psi = 10^{-2}$ and R_T is varied. (*b*) For the polarized endocytic trafficking mechanism, the dependence of cell speed on substratum adhesiveness is biphasic for small R_T but monophasic for large R_T. The range of adhesiveness permitting substantial migration speed widens with increasing R_T. Parameter values are the same as presented in Fig. 5 except $\theta = 10^{-3}$ and R_T is varied.

nism the range of adhesiveness permitting substantial migration speed is independent of R_T, whereas for the polarized endocytic trafficking mechanism increasing R_T dramatically widens the range of adhesiveness over which substantial migration speed can occur. Experiments in which cell speed is measured on substrata over a range of adhesiveness for cell populations possessing different levels of adhesion receptor expression thus might provide support for one of these mechanisms relative to the other.

Notice that the maximum cell speed is essentially independent of underlying asymmetry mechanism and of the asymmetry-generating parameters ψ and θ. Maximal speed occurs when cytoskeletal contraction disrupts all the uropodal bonds while leaving some lamellipodal bonds. Hence, net cell displacement is the same regardless of how this state is generated. It also should be pointed out that increasing directly cell-substratum adhesiveness, κ, can be achieved by either increasing the surface ligand density, n_s, or by decreasing the adhesion-receptor/ligand equilibrium dissociation constant, K_d, and thus increasing bond affinity. Therefore, if two different ligands possessing different affinities are compared, our model predicts that the cell speed curve should shift toward higher ligand densities for the lower affinity ligand.

Another critical requirement for one-dimensional cell movement is the generation of cytoskeletal contractile force. In Fig. 7 we plot cell speed vs. dimensionless contractile force generated f_c for different values of adhesiveness κ. Though this particular figure is based on the polarized endocytosis mechanism for bond asymmetry, these results and all the following results for the effects of cell rheological properties are independent of asymmetry-generating mechanism. Notice that cell speed also exhibits a biphasic dependence on contractile force. For low f_c no movement occurs because not enough force is generated to deform the cell and break adhesion bonds at either end of the cell. Increasing the contractile force increases cell speed as bonds are broken at the uropod but not the lamellipod, where there are more bonds to withstand contraction. This increase in speed is linear with f_c and continues until a maximum speed is reached. Further increases in contractile force result in the breakage of adhesion bonds at both ends of the cell as contraction just pulls front and back of the cell inwards. The critical value of f_c at which movement ceases depends on the adhesiveness κ: increasing κ produces more bonds at both ends of the cell and allows movement at higher values of f_c. Maximum speed is independent of adhesiveness above $\kappa \approx 10^{-1}$.

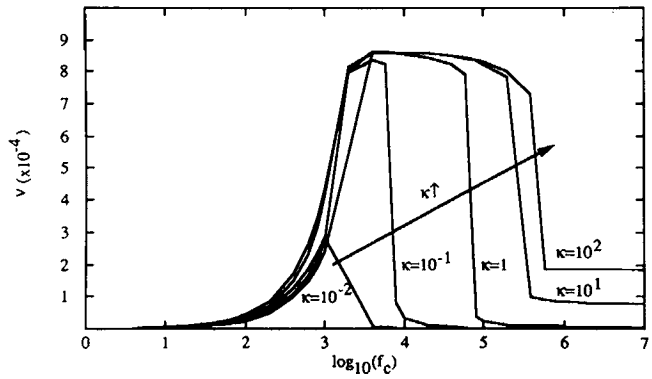

FIGURE 7 Model calculations for the effect of dimensionless intracellular contractile force f_c on dimensionless cell speed v for various dimensionless cell-substratum adhesivenesses κ. For significant cell speeds f_c must be great enough to break uropodal bonds and deform the cell but not too great so as to break all the lamellipodal bonds. At low κ contractile force generation results primarily in the breakage of bonds and cell movement is limited. Increasing adhesiveness allows the cell's bonds to withstand higher contractile forces and significant speeds will occur over a wider range of f_c. Maximum speed is independent of adhesiveness at high κ. Parameter values are as in Fig. 4 except $\psi = 1$, $\theta = 10^{-2}$, and f_c is varied.

The effect of contractile force on the bonds can be clearly seen by examining the forces transmitted by the bonds to the substratum at either end of the cell. Scaling Eq. 14 for the forces exerted on the bonds F_{bu} and F_{bl} with the spring force $\sqrt{k_{spring}k_bT}$, the dimensionless force on the bonds can be written as:

$$f_{bu} = \alpha\epsilon R_{bu}[\zeta_1(\tau_c)]\zeta_1(\tau_c) \tag{20a}$$

$$f_{bl} = \alpha\epsilon R_{bl}[\zeta_5(\tau_c)]\zeta_5(\tau_c). \tag{20b}$$

The total forces exerted to the substratum at the cell's back and front are, respectively:

$$F_u = c\left.\frac{du_1}{dt}\right|_{t=t_c} + k'u_1(t_c) + k_u u_1(t_c) \tag{21a}$$

$$F_l = -\left[c\left.\frac{du_5}{dt}\right|_{t=t_c} + k'u_5(t_c) + k_l u_5(t_c)\right]. \tag{21b}$$

Scaling these forces with the spring force yields:

$$f_u = \omega\left.\frac{d\zeta_1}{d\tau}\right|_{\tau=\tau_c} + \alpha\gamma_u[\zeta_1(\tau_c)]\zeta_1(\tau_c) \tag{22a}$$

$$f_l = -\left[\omega\left.\frac{d\zeta_5}{d\tau}\right|_{(\tau=\tau_c)} + \alpha\gamma_l[\zeta_5(\tau_c)]\zeta_5(\tau_c)\right]. \tag{22b}$$

Fig. 8 *a* shows how the fraction of total force exerted on the substratum by the bonds at the uropod varies with dimensionless contractile force for the adhesivities examined in Fig. 7, whereas Fig. 8 *b* shows the same relationship for the lamellipodal bonds. Because of asymmetry in bond distribution, the lamellipodal bonds

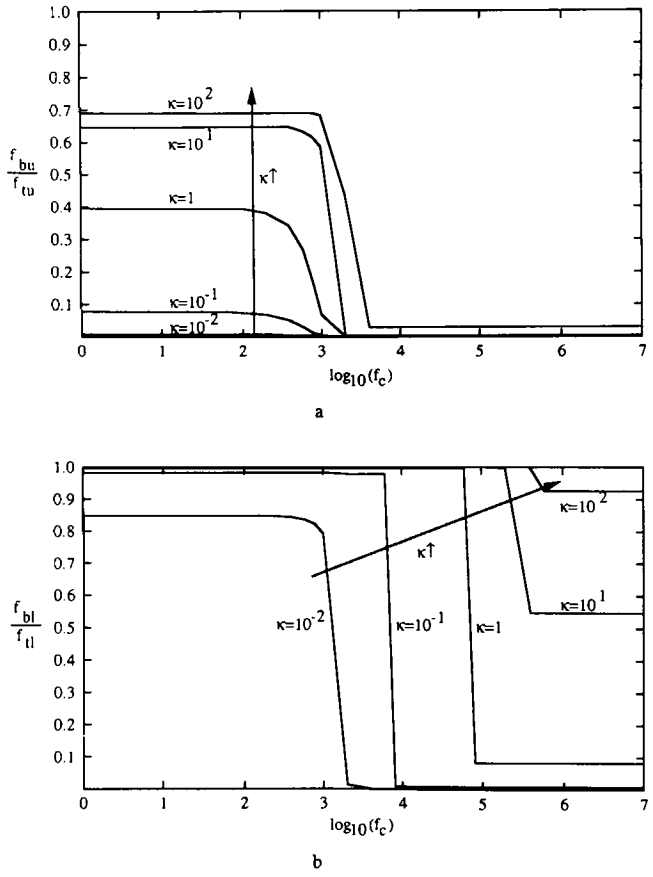

FIGURE 8 Comparison of bond traction force as a function of dimensionless intracellular contractile force f_c at different values of dimensionless cell-substratum adhesiveness κ between the front and rear of a moving cell. (*a*) Fraction of total force transmitted by adhesion bonds at the uropod f_{bu}/f_{tu} increases with increasing κ. Essentially independent of adhesiveness, a critical value of f_c is reached at which all the uropodal adhesion bonds fail and no longer support a portion of the traction force. (*b*) A corresponding plot for the fraction of force transmitted by adhesion bonds in the lamellipod f_{bl}/f_{tl}. Again increasing κ results in the transmission of a greater fraction of the traction force by the bonds, but now the critical force for bond failure depends on κ. Note also that the lamellipodal bonds support a greater fraction of the traction force than the uropodal bonds for positive bond numbers and that at high κ not all the bonds fail, even under large f_c. Parameter values are from Fig. 7.

always support a greater fraction of the transmitted force than the uropodal bonds. As adhesiveness is increased, the fraction of force supported by bonds at either end of the cell increases. Cell speed reaches a maximum at the value of contractile force at which the bonds at the uropod support a trivial fraction of the transmitted force, while the maximum value of f_c allowed for movement occurs when the lamellipodal bonds break and the fraction of force they exert drops dramatically. Note that at high adhesivities and moderate values of cell stiffness and viscosity the cell cannot effectively transmit enough force to break all the bonds in the front, so that cell speed does not decrease to zero as f_c is increased further.

Cell speed and the forces transmitted to the bonds and substratum depend not only on internal contractile force but also on the rheological properties of the cell and the contraction time force is exerted over. Fig. 9 demonstrates how cell speed varies with dimensionless stiffness α for different values of dimensionless viscosity ω. At low α, the cell is flaccid, deforms greatly under contraction, and little force can be transmitted to the bonds at either end of the cell: movement speed is small. Increasing α allows more efficient transmission of force to the bonds and movement is enhanced. However, as α is further increased, cell speed diminishes as the cell deforms minimally under contraction and the bonds become highly stressed. The effect of low α is, then, equivalent to the effect of low contractile force f_c, whereas high α is the equivalent of high f_c. At a given cell stiffness, increasing viscosity results in greater resistance to deformation and a decrease in cell speed.

The duration of the contraction phase of the movement cycle can have dramatic effects on maximum movement speed (computations not shown). Contraction time τ_c has little influence on cell speed for small contractile forces f_c, but has a great biphasic effect as f_c is increased. At short contraction times little movement occurs because the contractile force is not applied long enough to deform the cell and break uropodal bonds. Likewise, at long contraction times the contractile force

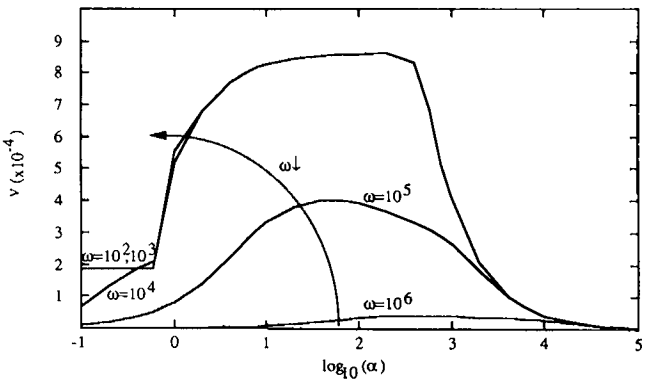

FIGURE 9 Relationship between cell rheology and cell movement speed is demonstrated in a plot of dimensionless speed ν vs. dimensionless cell stiffness α for various levels of dimensionless cell viscosity ω. At low α, the cell is flaccid and net movement is small; at high α, the cell is rigid and little movement can occur. An intermediate stiffness produces maximum speed. Increasing ω increases the cell's resistance to deformation and speed decreases monotonically. Parameter values are from Fig. 4 except $\kappa = 2$, $\psi = 1$, $\theta = 10^{-2}$, and α and ω are varied.

breaks the bonds at both ends of the cell before τ_c, resulting in no movement.

Comparison with experiments

The effect of substratum adhesiveness on movement speed has been the subject of two recent experimental studies. Goodman et al. (1989) examined the locomotion of murine skeletal muscle myoblasts over polystyrene surfaces coated with different amounts of laminin (Ln) and fibronectin (Fn) as well as the E8 (cell-binding) fragment of Ln. They found a biphasic relationship between movement speed and adsorbed protein concentration for Ln and E8, but speed increased slowly and monotonically for increasing surface densities of Fn over this range (Fig. 10 *a*). Speeds varied from 10 to 65 μ/h on Ln/E8 and from 10 to 20 μ/h on Fn. Using adhesion data from an earlier work (Goodman et al., 1987), in Fig. 10 *b* we plot speed against cell-substratum adhesive strength, measured as the fraction of cells which stably adhere at different protein concentrations. As expected, we see a biphasic dependence of movement speed with adhesiveness for LN and LN-fragment E8, with maxima in speed occurring at approximately one-third to one-half of the maximum adhesive strength, consistent with our hypothesis that an optimal adhesiveness exists for movement. Movement speed on FN, however, is small and increases only slowly through the regime of greatest adhesive strength.

Duband et al. (1989) examined the effect of substratum adhesive strength on the movement of embryonic neural crest cells (Fig. 11). Adhesiveness was varied by coating nontissue-culture petri dishes with increasing concentrations of Fn or antibodies possessing different affinities for the β1 subunit of FnR. While migration extent after 15 h decreased with increasing concentration of the high-affinity monoclonal ES46 and bivalent Ig 2999, migration was enhanced by increasing densities of the low-affinity monoclonals ES66 and JG22E as well as the monovalent Fab fragments of Ig 2999. ES46 and bivalent Ig 2999 have equilibrium dissociation constants on the order of 10^{-9} M, about two orders of magnitude lower than the K_d for Fn (Akiyama and Yamada, 1985). In contrast, monovalent Fab' 2999 has a K_d of roughly 10^{-7} M, and ES66 and JG22E have K_d's of 10^{-8} M. These observations can be interpreted using the model predictions presented in Figs. 4 or 5; at the adhesiveness, $\kappa_{max} = (n_s/K_d)_{max}$, for which maximal migration speed results, increases in ligand density must be compensated by decreases in receptor/ligand binding affinity. Hence, the data for the low-affinity ligands represent the increasing portion of the speed vs. adhesiveness curve, whereas the results for the high-affinity ligands represent the decreasing portion of the same curve.

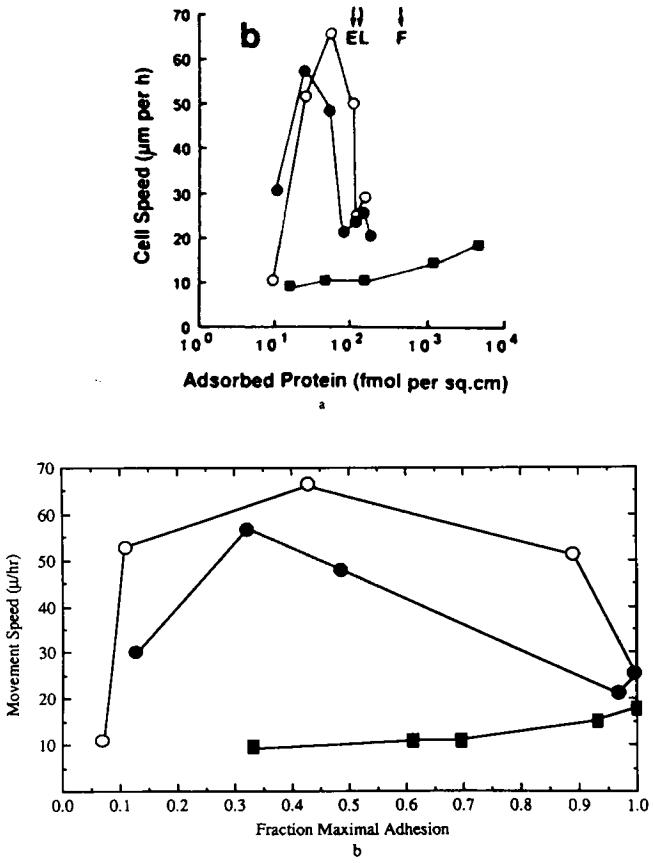

FIGURE 10 Cell speed of skeletal myoblasts migrating over polystyrene surfaces coated with the extracellular matrix proteins laminin (Ln) (*open circles*) and fibronectin (Fn) (*solid squares*) and a elastase-digestion fragment of Ln, E8 (*solid circles*) from Goodman et al. (1989). Speeds were measured using time-lapse videomicroscopy and image analysis. (*a*) Cell speed as a function of adsorbed protein density. Protein surface concentrations were measured by trace iodination and gamma counting. Movement speed demonstrated biphasic response on Ln and the E8 fragment, but increasing Fn density produced a slow and monotonic enhancement in speed over the concentration range examined. (*b*) Cell speed as a function of fraction of maximal adhesion. Adhesion data is from Goodman et al. (1987). Labeled myoblasts were added to appropriately coated chambers for 60 min at 37°C, nonadherent cells washed off, and adherent cells removed with trypsin/EDTA and counted. Fraction maximal adhesion is ratio of attachment efficiency (ratio of adherent to total cells added) at a given substrate concentration to maximum attachment efficiency. Cells on Ln migrated fastest at ~40% maximal adhesion, whereas cells on E8 exhibited maximum speed at ~30% maximal adhesion.

The effects of varying the force exerted by tissue cells during migration has been the subject of several experimental studies. For the most part, these studies have been qualitative in nature and reflect the properties of sheets of cells rather than individual cells (Bereiter-Hahn, 1987). Using deformable silicon rubber substrata, Danowski and Harris (1988) examined the simultaneous effects of the tumor promotor TPA (which transforms

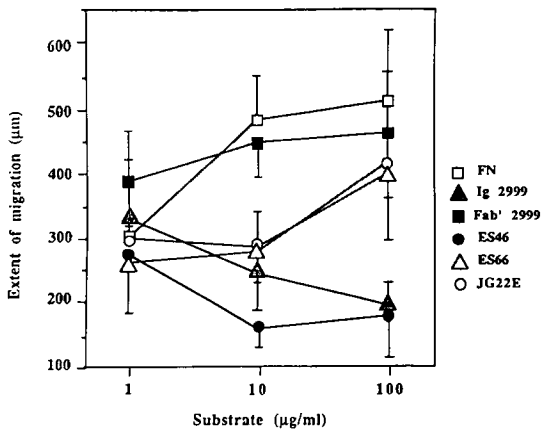

FIGURE 11 Data from Duband et al. (1989) examining the extent of migration of embryonic neural crest cells on ligand-coated nontissue culture petri dishes for a series of antibody ligands with different affinities for the β_1 subunit of fibronectin receptor. Extent of migration was measured as distance individual cells had moved after 15 h. Increasing concentrations of low-affinity monoclonal antibodies ES66 and JG22E enhance migration over the coating densities between 1 and 100 μg/ml, whereas the monoclonal ES46 and bivalent Ig2999 demonstrate the opposite trend. ES66 and Jg22E have approximately the same affinity for β_1 as Fn, but ES46 binds two order of magnitude more strongly. (Data shown appear in print in the recent publication; Duband, J.-L., S. Dufour, S. S. Yamada, K. M. Yamada, and J. P. Thiery. 1991. Neural crest cell locomotion induced by antibodies to β1 integrins. *J. Cell Sci.* 98:517–532.)

many cell types in culture) on contractility, adhesion, and migration of two fibroblast cell lines. Addition of TPA decreased the contractility of IMR-33 gerbil fibroma cells within minutes, as measured by loss of wrinkles in the rubber substratum. At the same time, TPA permitted these cells to attach to and migrate on normally nonadhesive plastic surfaces. These observations are consistent with previous work indicating that transformed cells adhere (Brown, 1988) and contract (Leader et al., 1983) more weakly than their nontransformed counterparts. Further, these results are in agreement with our model predictions. As Fig. 7 illustrates, decreasing the contractile force at high force levels can allow cells to move at nontrivial speeds on surfaces possessing lowered adhesiveness. This prediction may help explain why, in contrast to immotile cells, motile neural crest cells do not significantly distort silicone rubber substrata (Tucker et al., 1985). Immotile cells may generate force excessive for effective migration, whereas motile cells generate traction levels sufficient for movement but below the threshold measurable by this technique. However, because TPA may also modify FnR in CHO cells (Brown, 1988), further work is needed to demonstrate that transformation does not alter intrinsic cell-substratum adhesiveness.

Experimental approaches using rubber substrata measure forces exerted by the cells on their supporting surface, not directly the intracellular contractile force intrinsic to our model. Therefore, results of such experiments are more appropriately interpreted by comparison to model predictions for the dependence of cell speed on the traction force actually transmitted to the underlying substratum. The first question to address here is how the contractile force relates to the traction force. Because the cell pulls on both the lamellipod and the uropod, the net traction force is simply the sum of the total forces exerted at the front and back compartments of our model cell. In dimensionless form, this force is:

$$f_T = f_u + f_l = \omega \left.\frac{d(\zeta_1 - \zeta_5)}{d\tau}\right|_{\tau=\tau_c} + \alpha[\gamma_u\{\zeta_1(\tau_c)\}\,\zeta_1(\tau_c) - \gamma_l\{\zeta_5(\tau_c)\}\,\zeta_5(\tau_c)]. \quad (23)$$

Hence, the transmitted traction force depends implicitly on the intracellular contractile force, and explicitly on the cell rheological properties which govern the dissipation of the contractile force.

As noted earlier, a striking difference between immotile and motile cells in culture is the emphatic presence in the former of stress fibers. Nerem and co-workers examined the mechanical behavior and cytoskeletal organization of endothelial cells exposed to shear stress (Sato et al., 1987; Theret et al., 1988). They found that the formation of stress fibers was correlated with an increase in mechanical stiffness. Because it is reasonable to postulate that increases in stiffness are accompanied by increases in cell viscosity, for our analysis we define a new dimensionless viscoelastic parameter, $\bar{\omega}$:

$$\bar{\omega} = \frac{\omega}{\alpha} = \frac{\mu k_{ro}}{E}. \quad (24)$$

With this parameterization, by holding $\bar{\omega}$ constant we can explore the effects of increasing cell stiffness α while simultaneously increasing viscosity.

Fig. 12 illustrates how contractile force influences the traction force on the substratum for various levels of cell stiffness and viscosity. At low levels of force generation, traction increases linearly with contractile force. Changes in stiffness and viscosity have little effect in this regime. However, for greater intracellular forces, a maximum traction is reached. This maximum occurs because complete cell deformation limits the stress which can be exerted on the substratum. At low dimensionless stiffnesses maximum traction force increases monotonically with stiffness without complete breakage of adhesion bonds. However, for a stiffer and more viscous cell, all the adhesion bonds are broken at a critical dimensionless intracellular force (for the parameter combination depicted here $\sim 10^5$), resulting in a decrease in stress

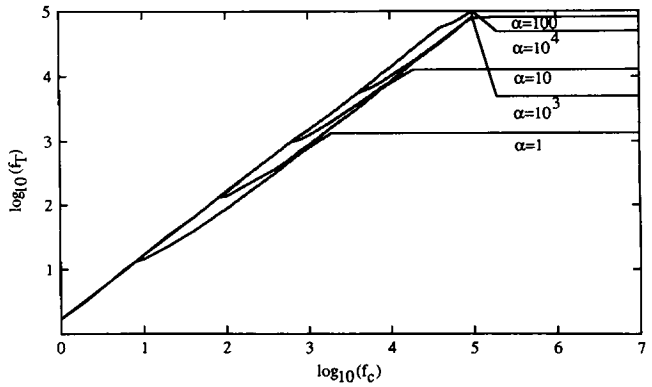

FIGURE 12 Effect of dimensionless intracellular contractile force f_c on dimensionless total traction force f_T exerted by both lamellipod and uropod for varying degrees of cell deformational resistance. Curves are parameterized for different values of dimensionless cell stiffness α holding $\bar{\omega}$ constant, so that increases in stiffness are accompanied by proportional increases in viscosity. f_T increases linearly with f_c for small f_c, relatively independent of α, up to a maximum total traction force that is exerted at complete cell deformation. Maximum traction force increases monotonically with α for α less than $\sim 10^2$. Resistance to deformation greater than this value results initially in a decrease in transmitted stress, but further increases in stiffness and viscosity limit this decrease. $\kappa = 2$, $\psi = 1$, $\theta = 10^{-3}$, $R_T = 6 \cdot 10^5$, $\eta = 10^{-5}$, $\delta = 10$, $\lambda = 0.333$, $\bar{\omega} = 1$, $\epsilon = 2 \cdot 10^{-3}$, $\sigma = 0.5$, $\tau_c = 180$, and $\beta = 0.5$.

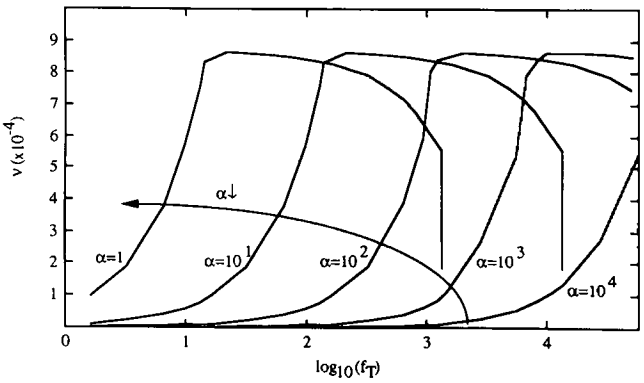

FIGURE 13 The relationship between dimensionless total traction force f_T and dimensionless cell speed v for different levels of cell stiffness and viscosity. Total traction force at a given value of f_c is calculated from Eq. 23 and plotted against v at the same value of f_c. Curves are parameterized as described in Fig. 12. Cell speed shows a biphasic dependence on F_T. Because a more resistant cell dissipates and transmits greater force without fully contracting, increases in α at constant $\bar{\omega}$ shift this curve toward higher f_T. Parameter values are the same as in Fig. 12.

transmitted to the surface. Further increases in stiffness and viscosity can limit this latter decrease.

We can use this information to investigate how cell speed varies with traction force for different levels of stiffness and viscosity (Fig. 13). Again cell speed exhibits a biphasic dependence on traction, for reasons analogous to the explanation of Fig. 7. Increasing the mechanical stiffness and viscosity of the cell shifts this curve toward higher force. A more rigid cell dissipates and transmits greater forces effectively without fully contracting.

These model predictions can be used to further intrepret the experimental results of Danowski and Harris (1988). Noting that leading lamellipodia become hyperextended upon addition of TPA, they concluded that this drug induces changes in cell mechanical properties. Although the rapid loss of contractility observed was not correlated with the immediate loss of focal adhesions, stress fibers were disrupted, in agreement with previous findings (Rifkin et al., 1979). Adding TPA, then, could reduce the traction force exerted on the underlying substratum simply by simultaneously decreasing the stiffness and viscosity of the cytoskeleton. The loss of stress fibers is equivalent to shifting left in Fig. 13 to a curve of decreased stiffness and viscosity, so that significant decreases in traction force still lead to increased motility. The effects of TPA on cell speed also will depend on whether it independently perturbs the actual contractile force generated.

SUMMARY

We have presented a simple mathematical model which relates basic cell biochemical and biophysical properties to cell movement speed, based on a chronological view of a cell migration "cycle" of lamellipodal extension, cytoskeletal contraction, and relaxation. This cell movement cycle is supported by observations of Trinkaus and others (Trinkaus, 1976; Lackie, 1986). Further, we hypothesize that the difference between the strength or number of adhesive interactions in the lamellipod and the uropod regulates cell speed. This theory is supported by recent work by Marks et al. (1991), who observed that the reduction in neutrophil movement speed on Fn-coated substrata upon inhibition of intracellular Ca^{2+} transients was due to an inability of the cells to detach at their uropods rather than an inability to extend lamellipodia, and that on less-adhesive substrata speed is further reduced because of poor lamellipodal traction.

By combining a viscoelastic-solid model describing cytoskeletal force generation and cell rheology with models for adhesion receptor trafficking and adhesion-receptor/ligand binding kinetics, we can predict the one-dimensional speed of cells on uniform, rigid substrata, such as petri dishes used in many in vitro studies

of cell migration. To allow generation of a stable polarized cell, we have examined two mechanisms which can result in an asymmetric distribution of adhesion bonds: polarized adhesion receptor trafficking, consisting of endocytosis and preferential insertion of recycled receptors at the leading edge, and spatial variations in strength of adhesion-receptor/ligand binding, which might occur with localized receptor proteolysis or phosphorylation at the cell's rear. As recently suggested (Aznavoorian et al., 1990), we have assumed in this present work that signal transduction events need not regulate the effects of adhesion on migration. Importantly, given reasonable estimates for cell adhesive and mechanical properties, a range of migration speeds consistent with typical observations for tissue cells (i.e., on the order of tens of microns per hour) can be predicted.

We have assumed that the generation of a net traction force on the underlying substrata, arising from intracellular cytoskeletal contraction and an asymmetric distribution of bonds linked to the cytoskeleton, drives cell migration. Our model does not invoke the hypothesis that membrane lipid flow produces cell movement (Bretscher, 1984). It is important to note that, by making no assumptions concerning bulk membrane flow, our model is consistent with recent observations for neutrophils, in which fluorescently tagged membrane components moved forward at the same velocity as the cell body during locomotion (Lee et al., 1990). Essentially, we have assumed that diffusion dominates transport of free receptors on the surface and that receptors bound to substratum ligand remain fixed with respect to the substratum. Hence, the convection in our model is that for the bound, fixed receptors with respect to the cell center-of-mass as the cell moves forward. We neglect any functional effects of receptor organization into aggregates, such as focal contacts, by cytoskeletal interactions, because little quantitative information exists concerning this phenomenon. The role of receptor organization in cell migration will be important to explore in future extensions of our model.

A major goal of our modeling approach is to generate clear predictions which can be tested experimentally. We predict that cell speed can exhibit a bimodal dependence on cell-substratum adhesiveness given either polarized receptor trafficking or spatial variations in adhesion-receptor/ligand affinity. However, as Fig. 6 demonstrates, distinctions can be found between these two alternative mechanisms. For the differential bond affinity mechanism, the dependence of cell speed on substratum adhesiveness is always biphasic regardless of adhesion receptor number R_T, and the range of adhesiveness permitting substantial migration speed is independent of R_T. For the polarized endocytic trafficking mechanism, the dependence of cell speed on substratum adhesiveness is biphasic for small R_T but monophasic for large R_T, and the range of adhesiveness permitting substantial migration speed widens with increasing R_T.

There exist several experimental approaches which may be able to distinguish between these postulated asymmetry-generating mechanisms. Immunofluorescence has been used to examine surface protein distributions on fibroblasts (Ishihara et al., 1988) and could be applied to determine if integrins accumulate at the front of a motile cell, as predicted for the polarized receptor trafficking mechanism. Alternatively, any effects of variations in adhesion receptor number on migration could be examined with cell subpopulations possessing different numbers of a particular integrin. Recently, two groups have isolated CHO cell populations either deficient in FnR expression (Schreiner et al., 1989) or transfected to increase FnR expression (Giancotti and Ruoslahti, 1990). With these cell systems, the model predictions for the alternative asymmetry mechanisms could be examined by measuring cell speed on surfaces coated with varying Fn ligand concentration. In reality, of course, multiple mechanisms for generating asymmetry may be acting simultaneously.

To truly understand how variations in contractile force and cell rheology affect movement, experimental systems must be designed which can carefully measure small forces and displacements associated with individual cell behavior. In general, the different feasible approaches, including well-characterized polymer films and silicone rubber and photoelastic sheets, measure traction forces exerted on a deformable surface rather than the intrinsic force generated intracellularly. However, even though our model analysis applies for movement stresses on rigid substrata, the traction forces predicted in Fig. 12 are comparable to the observations of James and Taylor (1969) for a single fibroblast. Drugs which disrupt the cytoskeleton, such as cytochalasin B, also could be used to determine the effects of changes in cellular rheology (Petersen et al., 1982). In conclusion, we hope that this present model, combined with experimental tools such as molecular biology, will motivate further studies to elucidate key factors and mechanisms in cell locomotion.

APPENDIX

Model analysis

To begin our analysis we scale the model equations so that they become dimensionless. Although cell length L is an obvious choice for a key length scale, the choice of time scale for dedimensionalization is less obvious. Three time scales are important. First, receptor dynamics

occur on the time scale of receptor-ligand dissociation, k_{ro}^{-1}. Cytoskeletal contraction occurs with a time constant of t_c, while the overall time scale of motion is on the order of the time required for one full movement cycle, t_m. To scale the equations with respect to a single key time scale, we scale time with respect to the smallest time scale k_{ro}^{-1}, so that $\tau = k_{ro}t$. This approach will be necessary in the future to analyze the full transient equations.

To scale the receptor trafficking Eqs. 2–6, we must remember that, in this one-dimensional model, receptor distributions will be symmetric with respect to the centerline along the length of the cell. Thus, we need only consider distributions for a half cell in our balances. Scaling the spatial coordinates with their appropriate maxima and receptor densities with the average receptor density for the cell, $R_T/2WL$, yields expressions for dimensionless cell length X, dimensionless cell width Y, and dimensionless receptor densities N_r^d, N_r^v, and N_b for dorsal free receptor, ventral free receptors, and bound receptors, respectively:

$$X = \frac{x}{L} \qquad Y = \frac{y}{L} \tag{A1}$$

$$N_r^d = \frac{2WLn_r^d}{R_T} \qquad N_r^v = \frac{2WLn_r^v}{R_T} \qquad N_b = \frac{2WLn_b}{R_T}. \tag{A2}$$

Along with the definition for dimensionless adhesiveness κ given by Eq. 15, we can define the following key dimensionless parameter groups:

$$\theta = \frac{k_e}{k_{ro}} \qquad \eta = \frac{D_r}{k_{ro}L^2} \qquad \delta = \frac{L}{W}. \tag{A3}$$

Cell speed, which is an unknown in this model, also can be scaled:

$$v = \frac{v}{k_{ro}L}. \tag{A4}$$

The balance equations for dorsal and ventral-free receptors (Eqs. 3a and 4a for the front λ and Eqs. 3b and 4b for the rear 1-λ of the cell), become:

$$\frac{\partial N_r^d}{\partial \tau} = \begin{cases} \eta\left[\frac{\partial^2}{\partial X^2} + \delta^2\frac{\partial^2}{\partial Y^2}\right]N_r^d - \theta N_r^d & \text{for } 0 \le X < 1-\lambda \\ \eta\left[\frac{\partial^2}{\partial X^2} + \delta^2\frac{\partial^2}{\partial Y^2}\right]N_r^d - \theta N_r^d & \\ \quad + \frac{\theta}{\lambda}\int_0^1\int_0^{1/2}(N_r^d + N_r^v)\,dYdX & \text{for } 1-\lambda \le X \le 1 \end{cases}. \tag{A5}$$

$$\frac{\partial N_r^v}{\partial \tau} = \begin{cases} \eta\left[\frac{\partial^2}{\partial X^2} + \delta^2\frac{\partial^2}{\partial Y^2}\right]N_r^v & \\ \quad -(\kappa+\theta)N_r^v + N_b & \text{for } 0 \le X < 1-\lambda \\ \eta\left[\frac{\partial^2}{\partial X^2} + \delta^2\frac{\partial^2}{\partial Y^2}\right]N_r^v - (\kappa+\theta)N_r^v + N_b & \\ \quad + \frac{\theta}{\lambda}\int_0^1\int_0^{1/2}(N_r^d + N_r^v)\,dYdX & \\ \text{for } 1-\lambda \le X \le 1 & \end{cases}. \tag{A6}$$

The mass balance for bound receptors over the entire ventral surface (Eq. 5) can now be written as:

$$\frac{\partial N_b}{\partial \tau} = \kappa N_r^v - N_b + v\frac{\partial N_b}{\partial X} \tag{A7}$$

with associated dimensionless boundary conditions:

$$N_r^d(X=0, Y) = N_r^v(X=0, Y) \tag{A8a}$$

$$N_r^d(X=1, Y) = N_r^v(X=1, Y) \tag{A8b}$$

$$N_r^d\left(X, Y=\frac{1}{2}\right) = N_r^v\left(X, Y=\frac{1}{2}\right) \tag{A8c}$$

$$\left.\frac{\partial(N_r^d + N_r^v)}{\partial Y}\right|_{X,Y=1/2} = 0 \tag{A8d}$$

$$\left.\frac{\partial N_r^d}{\partial Y}\right|_{X,Y=0} = 0 \tag{A8e}$$

$$\left.\frac{\partial N_r^v}{\partial Y}\right|_{X,Y=0} = 0 \tag{A8f}$$

$$\left.\frac{\partial(N_r^d + N_r^v)}{\partial X} - vN_b\right|_{X=0,Y} = 0 \tag{A8g}$$

$$\left.\frac{\partial(N_r^d + N_r^v)}{\partial K} + vN_b\right|_{X=1,Y} = 0. \tag{A8h}$$

Note that for the half cell the fluxes of each individual free receptor species (dorsal and ventral) across the cell's centerline must be zero.

Finally, conservation of receptors still applies:

$$\int_0^1\int_0^{1/2}(N_r^d + N_r^v + N_b)\,dYdX = 1. \tag{A9}$$

To simplify scaling of the equations describing cytoskeletal contraction (Eqs. 8, 9, 15, and 18), it is helpful to define viscoelastic parameters which depend only on the intrinsic cell stiffness and viscosity and can be estimated for individual cells. If, in addition to our supposition of homogeneity, we assume that the cell is isotropic and deformations are small, the elasticity will be uniform throughout the cell and characterized by a Young's modulus E, defined as the linear proportionality between stress and strain. The Hookean spring constants k, k', and k_c can then be simply related to the Young's modulus and characteristic length $L/6$ by assuming an appropriate cross-sectional area for each element:

$$k = \frac{6A_{body}E}{L} \qquad k' = \frac{6A_{end}E}{L} \qquad k_c = \frac{6A_{bond}E}{L}. \tag{A10}$$

A_{body} represents the cross-sectional area of the cell body. A_{end} is an effective cross-sectional area for the cytoskeletal element in the pseudopodal compartments not connected to bonds, whereas A_{bond} is the effective cross-sectional area of a cytoskeletal element connected to a bond. Similarly, the behavior of the dashpots can be characterized by a viscosity coefficient μ, which is the proportionality constant between stress and rate of strain. The dashpot constant c is proportional to μ:

$$c = \frac{6A_{body}\mu}{L}. \tag{A11}$$

Finally, assuming each cell body compartment generates a uniform

force $F_c = F_i (i = 2, \ldots, 5)$ in both time and space, we scale each node displacement with compartment length and force with the spring force $\sqrt{k_{spring} k_b T}$:

$$\zeta_i = \frac{6u_i}{L} \qquad f_c = \frac{F_c}{\sqrt{k_{spring}\, k_b T}}. \tag{A12}$$

Defining dimensionless parameters α, ω, ϵ, and σ characterizing cell viscoelasticity:

$$\alpha = \frac{A_{body} E}{\sqrt{k_{spring}\, k_b T}} \tag{A13a}$$

$$\omega = \frac{A_{body}\, \mu k_{ro}}{\sqrt{k_{spring}\, k_b T}} \tag{A13b}$$

$$\epsilon = \frac{A_{bond}}{A_{body}} \tag{A13c}$$

$$\sigma = \frac{A_{end}}{A_{body}} \tag{A13d}$$

the node displacement matrix Eq. 18 becomes:

$$\frac{d}{d\tau}\begin{bmatrix}\zeta_1\\ \zeta_2\\ \zeta_3\\ \zeta_4\\ \zeta_5\end{bmatrix} = -\frac{\alpha}{\omega}\begin{bmatrix} \frac{5\gamma_u(\zeta_1)+1}{6} & 0 & 0 & 0 & \frac{\gamma_l(\zeta_5)-1}{6} \\ \frac{2[\gamma_u(\zeta_1)-1]}{3} & 1 & 0 & 0 & \frac{\gamma_l(\zeta_5)-1}{3} \\ \frac{\gamma_u(\zeta_1)-1}{2} & 0 & 1 & 0 & \frac{\gamma_l(\zeta_5)-1}{2} \\ \frac{\gamma_u(\zeta_1)-1}{3} & 0 & 0 & 1 & \frac{2[\gamma_l(\zeta_5)-1]}{3} \\ \frac{\gamma_u(\zeta_1)-1}{6} & 0 & 0 & 0 & \frac{5\gamma_l(\zeta_5)+1}{6} \end{bmatrix} \cdot \begin{bmatrix}\zeta_1\\ \zeta_2\\ \zeta_3\\ \zeta_4\\ \zeta_5\end{bmatrix} + \frac{F_c}{3\omega}\begin{bmatrix}2\\ 1\\ 0\\ -1\\ -2\end{bmatrix}. \tag{A14}$$

The ratio of total pseudopod stiffness to cell body stiffness γ for each pseudopod will be a function of bond number in the terminal compartments and can be expressed as:

$$\gamma_u[\zeta_1(\tau)] = \sigma + \epsilon R_{bu}[\zeta_1(\tau)] = \sigma + \frac{\epsilon R_T \int_0^{1/6}\int_0^{1/2} (N_r^v + N_b)\, dYdX}{1 + \psi\kappa^{-1} e\{[\epsilon\alpha\zeta_1(\tau)]^2\}} \tag{A15a}$$

$$\gamma_l[\zeta_5(\tau)] = \sigma + \epsilon R_{bl}[\zeta_5(\tau)] = \sigma + \frac{\epsilon R_T \int_{5/6}^{1}\int_0^{1/2} (N_r^v + N_b)\, dYdX}{1 + \kappa^{-1} e\{[\epsilon\alpha\zeta_5(\tau)]^2\}}. \tag{A15b}$$

Each node starts at its origin and is constrained to remain within the cell body:

$$\zeta_i(\tau = 0) = 0 \tag{A16a}$$

$$-i \le \zeta_i(\tau) \le 6 - i \quad i = 1, \ldots, 5 \tag{A16b}$$

and the cell contracts for a dimensionless time $\tau_c = k_{ro} t_c$.

Defining β as the fraction of movement cycle time the cell spends in the contraction phase:

$$\beta = \frac{t_c}{t_m} \tag{A17}$$

the overall dimensionless velocity v of the cell can be expressed in terms of dimensionless variables from the viscoelastic-solid model:

$$v = \frac{\beta \sum_{i=1}^{5} \zeta_i(\tau = \tau_c)}{30\tau_c}. \tag{A18}$$

Parameter estimates

Estimates of dimensional parameters in our model for tissue cells are presented in Table A1. The rate constant for receptor-ligand bond formation can be estimated by assuming that bond formation is diffusion limited in the membrane (Bell, 1978):

$$k_f = 2\pi D_r \tag{A19}$$

with D_r receptor diffusivity in the cell membrane. The rate constant for unstressed bond dissociation, k_{ro}, can then be calculated using literature values of the equilibrium dissociation constant K_d measured for soluble ligand, assuming that the rate of binding of soluble ligand to membrane-bound receptor also is diffusion limited (Lauffenburger, 1989). Jacobson and co-workers have found that the diffusivity of integrins is comparable to diffusivities for other membrane proteins (Duband et al., 1988*b*). Finally, several investigators have measured similar internalization rates using monoclonal antibodies for an integrin or its β subunit (Bretscher, 1989; Raub and Kuentzel, 1989; Sczekan and Juliano, 1990).

Estimating the key parameters describing cell rheology and the contractile process is more difficult. Whole-cell techniques, such as micropipette aspiration and particle diffusion (Bereiter-Hahn, 1987), have been most successfully applied to measure the viscosity of white blood cells (Evans and Yeung, 1989). Similar measurements for adherent tissue cells are less established, and, accordingly, we base our estimates of tissue cell rheology on measurements made of polymerized F-actin (Sato et al., 1987; Zaner and Valberg, 1989). The elasticity of F-actin has been measured as a modulus of rigidity G, which, assuming incompressibility, can be easily related to the Young's modulus (Fung, 1977);

$$E = 3G. \tag{A20}$$

The pseudopods of spread cells (i.e., in the presence of adhesion bonds) should be stiffer than the cell body (Schmid-Schoenbein et al., 1982), while in the absence of bonds, cells do not spread and the cell body should be stiffer than the pseudopods. These suppositions are equivalent to:

$$\gamma_i[R_{bi} > 0] = \sigma + \epsilon R_{bi} > 1 \quad \text{and } \gamma_i[R_{bi} = 0] = \sigma < 1 \quad i = u \text{ or } l. \tag{A21}$$

Choices for σ and ϵ are predicated on satisfying these two conditions for resonable bond numbers; model predictions are relatively insensitive to either parameter (computations not shown). Finally, contractile forces generated can be estimated from observations of the cells on deformable silicone rubber (Harris et al., 1980).

TABLE A1 **Dimensional parameter estimates**

Parameter	Definition	Range	Reference
K_d	Equilibrium dissociation constant	10^{-6}–$10^{-8}\ M^{-1}$	Horwitz et al. (1985), Akiyama and Yamada (1985), Dejana et al. (1988)
R_T	Receptor number	10^4–10^7	Akiyama and Yamada (1985), Dejana et al. (1988), Sczekan and Juliano (1990)
k_e	Endocytosis rate	10^{-6}–$10^{-2}\ s^{-1}$	Bretscher (1989), Raub and Kuentzel (1989), Sczekan and Juliano (1990)
D_r	Receptor diffusivity	10^{-9}–$10^{-12}\ \frac{cm^2}{s}$	Jacobson et al. (1987), Duband et al. (1988*b*)
n_s	Substratum ligand density	10^7–$10^{13}\ \frac{molecules}{cm^2}$	Goodman et al. (1989)
F_c	Force generated	10^{-2}–10^{-6} dyn per compartment	Harris et al. (1980), James and Taylor (1969)
E	Elasticity	1–$10^3\ \frac{dyn}{cm^2}$	Sato et al. (1987), Zaner and Valberg (1989)
μ	Viscosity	10^2–10^5 poise	Bereiter-Hahn (1987)
k_{spring}	Bond spring constant	$10^{-1}\ \frac{dyn}{cm^2}$	Bell et al. (1984)
L	Cell length	25–100 μ	Trinkaus (1984)
W	Cell width	2–20 μ	Trinkaus (1984)
A_{body}	Cross-sectional area of cell body	1–50 μ^2	Trinkaus (1984)
t_c	Contraction time	$6 \cdot 10^1$–$6 \cdot 10^3\ s$	Trinkaus (1984), Chen (1981)
t_m	Movement cycle time	10^2–$10^4\ s$	Trinkaus (1984), Chen (1981)

Numerical solution procedure

The equations which describe the adhesion receptor dynamics and viscoelastic-solid models are highly coupled: receptor distribution depends on cell speed, which in turn depends on the number of receptors in the ventral face of the lamellipod and uropod and thus, receptor distribution. Assuming that the kinetics of receptor/ligand binding are faster than the kinetics of contraction, receptor distribution will reach steady state during lamellipod extension and cytoskeletal relaxation (Lauffenburger, 1989), which is equivalent to setting Eqs. A5–A7 to zero. In this work, we assume that this steady-state receptor trafficking assumption is valid and neglect the influence of cell speed on receptor distribution, allowing the systems of Eqs. A5–A9, A14–A16, and A18 to be uncoupled. This approach is reasonable for large adhesion bond asymmetries, as would be generated by movement at low adhesiveness, low cell speed, high rates of endocytosis, or large differences in affinity between the front and back of the cell. The solution of the full transient equations necessary to describe one-dimensional cell movement at high speeds will be the subject of a subsequent paper. With velocity set to zero, we solve for receptor distribution as a function of κ, θ, η, λ, and δ using a finite difference approach in which the half-cell problem is discretized into a grid of 40 by 10 elements. The finite difference equations are solved using LINPACK (Dongarra et al., 1979). Using the resulting dimensionless receptor distribution the dimensionless node displacement equations are integrated over a dimensionless time τ_c using LSODE (Hindmarsh, 1981) and velocity found from Eq. A18. A schematic illustration of this solution procedure is given in Fig. A1.

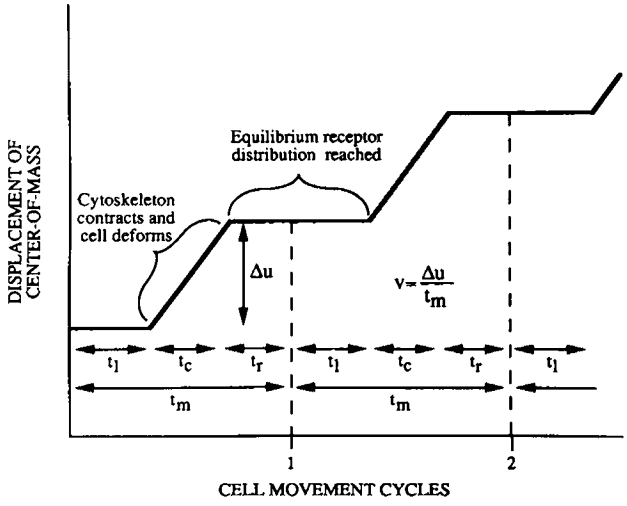

FIGURE A1 Schematic illustration of solution procedure. With $v = 0$, Eqs. A5–A9 at steady state are solved for the receptor distribution in absence of cytoskeletal contraction. Eqs. A14–A16 are then integrated to obtain node displacements between cell compartments. Eq. A18 yields the overall cell velocity.

Our approach is valid for low values of the adhesiveness parameter κ, as can be seen in a plot of receptor asymmetry ρ vs. dimensionless speed v at different values of κ (Fig. A2). ρ is defined at the ratio of total ventral receptors in the lamellipod to uropod:

$$\rho = \frac{\int_{5/6}^{1}\int_{0}^{1/2}(N_r^v + N_b)\,dYdX}{\int_{0}^{1/6}\int_{0}^{1/2}(N_r^v + N_b)\,dYdX}. \qquad \text{(A22)}$$

At low adhesiveness few receptors bind to the substratum and the convection of bound receptors toward the tail of the cell, due to forward cell movment, affects only a small fraction of the total number of ventral receptors. However, as adhesiveness is increased, the

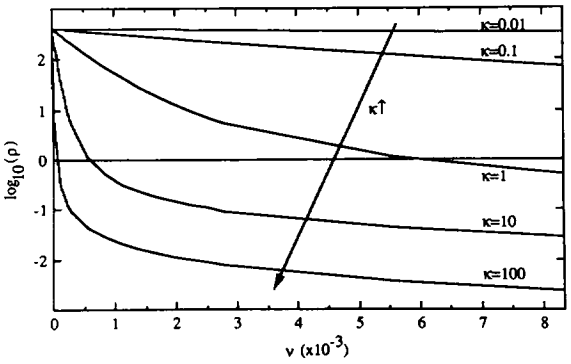

FIGURE A2 Effect of dimensionless speed ν on adhesion receptor asymmetry at various levels of dimensionless cell-substratum adhesiveness κ. Receptor asymmetry is represented by ρ, the ratio of total lamellipodal receptors to total uropodal receptors on the ventral surface. The model requires values of ρ greater than unity to generate a net traction force and cell translocation in the forward direction. At low degrees of adhesiveness κ, cell speed has little effect on receptor asymmetry, but increasing κ limits the movement speed for which positive receptor asymmetry ($\rho > 1$) exists. These curves were determined by solving Eqs. A5–A9 and A22 using a finite difference approach. $\theta = 5.56 \cdot 10^{-3}$, $\eta = 1.33 \cdot 10^{-5}$, $\delta = 10$, and $\lambda = 0.333$.

number of bound receptors become larger and convection affects more receptors. A point is finally reached at which the rearward convection of bound receptors overcomes the forward transport of unbound receptors through endocytosis/insertion and no adhesion receptor asymmetry results ($\rho = 1$). The same effect occurs as the cell moves faster (ν increases), either at constant adhesiveness or if bond asymmetry is generated by differences in adhesiveness between front and rear of the cell, and results from the breakdown of the steady-state receptor trafficking assumption. The value of ν at which $\rho = 1$, ν_c, depends on the parameters describing receptor distribution (κ, θ, η, λ, δ, and ψ). Increases in dimensionless adhesiveness κ result in nearly reciprocal decreases in critical cell speed ν_c, whereas greater dimensionless endocytosis rates θ increase ν_c at constant κ (computations not shown).

We would like to thank T. Kyle Vanderlick for the use of a Sun 4 SPARCstation for numerical computations and J. A. Quinn for many helpful discussions.

This works has been partially supported by National Institute of Health grant GM-41476 to Dr. Lauffenburger and a grant from the Whitaker Foundation and a National Science Foundation Graduate Student Fellowship to P. DiMilla.

Received for publication 24 August 1990 and in final form 14 March 1991.

REFERENCES

Akiyama, S. K., and K. M. Yamada. 1985. The interaction of plasma fibronectin with fibroblastic cells in suspension. *J. Biol. Chem.* 260:4492–4500.

Aznavoorian, S., M. L. Stracke, H. Knutzsch, E. Schiffman, and L. A. Liotta. 1990. Signal transduction for chemotaxis and haptotaxis by matrix molecules in tumor cells. *J. Cell Biol.* 110:1427–1438.

Bell, G. I. 1978. Models for the specific adhesion of cells to cells. *Science (Wash. DC).* 200:618–627.

Bell, G. I., M. Dembo, and P. Bongrand. 1984. Cell adhesion. Competition between nonspecific repulsion and specific bonding. *Biophys. J.* 45:1051–1064.

Bereiter-Hahn, J. 1987. Mechanical principles of architecture of eukaryotic cells. *In* Cytomechanics. The Mechanical Basis of Cell Form and Structure. J. Bereiter-Hahn, O. R. Anderson, and W.-E. Reif, editors. Springer-Verlag, Berlin. 3–30.

Bongrand, P., and G. I. Bell. 1984. Cell-cell adhesion: parameters and possible mechanisms. *In* Cell Surface Dynamics: Concepts and Models. A. S. Perelson, C. DeLisi, and F. Wiegel, editors. Marcel Dekker, Inc., New York. 459–493.

Bretscher, M. 1984. Endocytosis: relation to capping and cell locomotion. *Science (Wash. DC).* 224:681–686.

Bretscher, M. S. 1989. Endocytosis and recycling of the fibronectin receptor in CHO cells. *EMBO J. (Eur. Mol. Biol. Organ.)* 8:1341–1348.

Brown, P. J. 1988. Phorbol ester stimulation of fibronectin-mediated cell adhesion. *Biochem. Biophys. Res. Commun.* 155:603–607.

Buck, C. A., and A. F. Horwitz. 1987. Cell surface receptors for extracellular matrix molecules. *Annu. Rev. Cell Biol.* 3:179–205.

Burridge, K., K. Faith, T. Kelly, G. Nuckolls, and C. Turner. 1988. Focal adhesions: transmembrane junctions between the extracellular matrix and the cytoskeleton. *Annu. Rev. Cell Biol.* 4:487–525.

Carter, S. B. 1965. Principles of cell motility: the direction of cell movement and cancer metastasis. *Nature* (Lond.). 213:256–260.

Chen, W.-T. 1981. Surface changes during retraction-induced spreading of fibroblasts. *J. Cell. Sci.* 49:1–13.

Danowski, B. A., and A. K. Harris. 1988. Changes in fibroblast contractility, morphology, and adhesion in response to a phorbol ester tumor promoter. *Exp. Cell Res.* 177:47–59.

Dejana, E., G. Conforti, A. Zanetti, L. Languino, and P. Marchiso. 1988. Structure and organization of adhesion receptors in endothelial cells. *Presented at the Vth International Symposium on the Biology of the Vascular Endothelial Cell, Toronto.*

Dembo, M., F. H. Harlow, and W. Alt. 1984. The biophysics of cell motility. *In* Cell Surface Dynamics: Concepts and Models. A. S. Perelson, C. DeLisi, and F. Weigel, editors. Marcel Dekker, Inc., New York. 495–542.

Dembo, M., L. Tuckerman, and W. Goad. 1981. Motion of polymorphonuclear leukocytes: theory of receptor redistribution and the frictional force on a moving cell. *Cell Motil.* 1:205–235.

Dembo, M., D. C. Torney, K. Saxman, and D. Hammer. 1988. The reaction-limited kinetics of membrane-to-surface adhesion and detachment. *Proc. Roy. Soc. Lond. B.* 234:55–83.

Devreotes, P. N., and S. H. Zigmond. 1988. Chemotaxis in eukaryotic cells: a focus on leukocytes and *Dictyostelium*. *Annu. Rev. Cell Biol.* 4:649–686.

Dong, C., R. Skalak, K.-L. P. Sung, G. W. Schmid-Schonbein, and S. Chien. 1988. Passive deformation analysis of human leukocytes. *J. Biomech. Eng.* 110:27–36.

Dongarra, J. J., J. R. Bunch, C. B. Moler, and G. W. Stewart. 1979. LINPACK. Argonne National Laboratory.

Duband, J.-L., S. Dufour, and J. P. Thiery. 1988*a*. Extracellular matrix-cytoskeleton interactions in locomoting embryonic cells. *Protoplasma.* 145:112–119.

Duband, J.-L., G. H. Nuckolls, A. Ishihara, T. Hasegawa, K. M.

Yamada, J. P. Thiery, and K. Jacobson. 1988*b*. Fibronectin receptor exhibits high lateral mobility in embryonic locomoting cells but is immobile in focal contacts and fibrillar streaks in stationary cells. *J. Cell Biol.* 107:1385–1396.

Duband, J.-L., S. Dufour, and J. P. Thiery. 1989. Migration-promoting effect of fibronectin is mimicked by antibodies to integrins with moderate affinity. *J. Cell Biol.* 109:76*a*. (Abstr.).

Evans, E., and A. Yeung. 1989. Apparent viscosity and cortical tension of blood granulocytes determined by micropipette aspiration. *Biophys. J.* 56:151–160.

Fung, Y. C. 1977. A First Course in Continuum Mechanics. Prentice-Hall, Inc., Englewood Cliffs, NJ.

Gailit, J., and E. Ruoslahti. 1988. Regulation of the fibronectin receptor affinity by divalent cations. *J. Biol. Chem.* 263:12927–31292.

Giancotti, P., and E. Ruoslahti. 1990. Elevated levels of the α5β1 fibronectin receptor suppress the transformed phenotype of Chinese hamster ovary cells. *Cell.* 60:849–859.

Goodman, S. L., R. Deutzmann, and K. von der Mark. 1987. Two distinct cell-binding domains in laminin can independently promote nonneuronal cell adhesion and spreading. *J. Cell Biol.* 105:589–598.

Goodman, S. L., G. Risse, and K. von der Mark. 1989. The E8 subfragment of laminin promotes locomotion of myoblasts over extracellular matrix. *J. Cell Biol.* 109:799–809.

Gotlieb, A. I., L. McBurnie May, L. Subrahmanyan, and V. I. Kalnins. 1981. Distribution of microtubule organizing centers in migrating sheets of endothelial cells. *J. Cell Biol.* 91:589–594.

Grinnell, F. 1986. Focal adhesion sites and the removal of substratum-bound fibronectin. *J. Cell Biol.* 103:2697–2706.

Harris, A. K. 1973. Behavior of cultured cells on substrata of variable adhesiveness. *Exp. Cell Res.* 77:285–297.

Harris, A. K., P. Wild, and D. Stopak. 1980. Silicone rubber substrata: a new wrinkle in the study of cell locomotion. *Science (Wash. DC).* 208:177–179.

Heath, J. 1983. Behavior and structure of the leading lamella in moving fibroblasts: occurrence and centripetal movement of arc-shaped microfilament bundles beneath the dorsal cell membrane. *J. Cell Sci.* 60:331–354.

Hindmarsh, A. 1981. LSODE: Livermore solver for ordinary differential equations. Lawrence Livermore Labs.

Hirst, R., A. Horwitz, C. Buck, and L. Rohrschneider. 1986. Phosphorylation of the fibronectin receptor complex in cells transformed by oncogenes that encode tyrosine kinases. *Proc. Natl. Acad. Sci. USA.* 83:6470–6474.

Horwitz, A. F., K. Duggan, C. Buck, M. C. Beckerle, and K. Burridge. 1986. Interaction of plasma membrane fibronectin receptor with talin. A transmembrane linkage. *Nature (Lond.).* 320:531–532.

Hynes, R. O. 1987. Integrins: a family of cell surface receptors. *Cell.* 48:549–554.

Ishihara, A., B. Holifield, and K. Jacobson. 1988. Analysis of lateral redistribution of a monoclonal antibody complex plasma membrane glycoprotein which occurs during cell locomotion. *J. Cell Biol.* 106:329–343.

Jacobson, K., A. Ishihara, and R. Inman. 1987. Lateral diffusion of proteins in membranes. *Annu. Rev. Physiol.* 49:163–175.

James, D. W., and J. F. Taylor. 1969. The stress developed by sheets of chick fibroblasts in vitro. *Exp. Cell Res.* 54:107–110.

Lackie, J. M. 1986. Cell Movement and Cell Behavior. Allen and Unwin, London.

Lackie, J. M., and P. C. Wilkinson. 1984. Adhesion and locomotion of neutrophil leukocytes on 2-D substrata and 3-D matrices. *In* White Blood Cell Mechanics: Basic Science and Clinical Aspects. H. J. Meiselman, M. A. Lichtman, and P. L. LaCelle, editors. Alan R. Liss, New York. 237–254.

Lauffenburger, D. 1989. A simple model for the effects of receptor-mediated cell-substratum adhesion on cell migration. *Chem. Eng. Sci.* 44:1903–1914.

Leader, W. M., D. Stopak, and A. K. Harris. 1983. Increased contractile strength and tightened adhesion to the substratum result from reverse transformation of CHO cells by dibutyrl cyclic adenosine monophosphate. *J. Cell Sci.* 64:1–11.

Lee, J., M. Gustafsson, K.-E. Magnusson, and K. Jacobson. 1990. The direction of membrane lipid flow in locomoting polymorphonuclear leukocytes. *Science (Wash. DC).* 247:1229–1233.

Marks, P. W., B. Hendley, and F. R. Maxfield. 1991. Attachment to fibronectin or vitronectin makes human neutrophil migration sensitive to alterations in cytosolic free calcium concentration. *J. Cell Biol.* 112:149–158.

Mueller, S. C., T. Kelly, M. Dai, H. Dai, and W.-T. Chen. 1989. Dynamic cytoskelton-integrin associations induced by cell binding to immobilized fibronectin. *J. Cell Biol.* 109:3455–3464.

Oster, G. F., and A. S. Perelson. 1987. The physics of cell motility. *J. Cell Sci.* 8:35–54.

Petersen, L. O., W. B. McConnaughey, and E. L. Elson. 1982. Dependence of locally measured cellular deformability on position of cell, temperature, and cytochalasin B. *Proc. Natl. Acad. Sci. USA.* 79:5327–5331.

Raub, T. J., and S. L. Kuentzel. 1989. Kinetic and morphological evidence for endocytosis of mammalian cell integrin receptors by using an anti-fibronectin receptor β subunit monoclonal antibody. *Exp. Cell Res.* 184:407–426.

Rifkin, D. B., R. M. Crowe, and R. Pollack. 1979. Tumor promotors induce changes in the chick-embryo fibroblast cytoskeleton. *Cell.* 18:361–368.

Ruoslahti, E., and M. D. Pierschbacher. 1987. New perspectives in cell adhesion: RGD and integrins. *Science (Wash. DC).* 238:491–497.

Sato, M., M. J. Levesque, and R. M. Nerem. 1987. Micropipette aspiration of cultured bovine aortic endothelial cells exposed to shear stress. *Atherosclerosis.* 7:276–285.

Sato, M., W. H. Schwarz, and T. D. Pollard. 1987. Dependence of the mechanical properties of actin/α-actinin gels on deformation rate. *Nature (Lond.).* 325:828–830.

Schmid-Schonbein, G. W., K.-L. P. Sung, A. Tozeren, R. Skalak, and S. Chien. 1981. Passive mechanical properties of human leukocytes. *Biophys. J.* 36:243–256.

Schmid-Schonbein, G. W., R. Skalak, K.-L. P. Sung, and S. Chien. 1982. Human leukocytes in the active state. *In* White Blood Cells: Morphology and Rheology as Related to Function. U. Bagge, G. V. R. Born, and P. Gaehtgens, editors. Martinus Nijhoff Publishers, the Hague, the Netherlands. 21–31.

Schreiner, C. L., J. S. Bauer, Y. N. Danilov, S. Hussein, M. M. Sczekan, and R. L. Juliano. 1989. Isolation and characterization of Chinese hamster ovary cell variants in the expression of fibronectin receptor. *J. Cell Biol.* 109:3157–3167.

Sczekan, M. M., and R. L. Juliano. 1990. Internalization of the fibronectin receptor is a constitutive process. *J. Cell. Phys.* 142:575–580.

Singer, S., and A. Kupfer. 1986. The directed migration of eukaryotic cells. *Annu. Rev. Cell Biol.* 2:337–365.

Stossel, T., C. Chapponnier, R. Ezzell, J. Hartwig, and P. Janney. 1985. Nonmuscle actin-binding proteins. *Annu. Rev. Cell Biol.* 1:353–402.

Tapley, P., A. Horwitz, C. Buck, K. Duggan, and L. Rohrschneider. 1989. Integrins isolated from Rous sarcoma virus-transformed chicken embryo fibroblasts. *Oncogene.* 4:325–333.

Theret, D. P., M. J. Levesque, M. Sato, R. M. Nerem, and L. T. Wheeler. 1988. The application of a homogeneous half-space model in the analysis of endothelial cell micropipette measurements. *J. Biomech. Eng.* 110:190–199.

Trinkaus, J. P. 1976. On the mechanism of multicellular cell movements. *In* The Cell Surface in Animal Embryogenesis and Development. G. Poste and G. L. Nicholson, editors. Elsevier/North Holland, Amsterdam. 1–25.

Trinkaus, J. P. 1984. Cells Into Organs. The Forces That Shape the Embryo. Prentice-Hall, Inc., Englewood Cliffs, NJ.

Tucker, R. P., B. F. Edwards, and C. A. Erickson. 1985. Tension in the culture dish: microfilament organization and migratory behavior of quail neural crest cells. *Cell Motil.* 5:225–237.

Zahalak, G. I., W. B. McConnaughey, and E. L. Elson. 1990. Determination of cellular mechanical properties by cell poking, with an application to leukocytes. *J. Biomech. Eng.* 112:283–294.

Zaner, K. S., and P. A. Valberg. 1989. Viscoelasticity of F-actin measured with magnetic microparticles. *J. Cell. Biol.* 109:2233–2243.

Zhu, C., and R. Skalak. 1988. A continuum model of protrusion of pseudopod in leukocytes. *Biophys. J.* 54:1115–1137.

Zhurkov, S. N. 1965. Kinetic concept of strength of solids. *Int. J. Frac. Mech.* 1:311–323.